Spatial-temporal heterogeneity of magma emplacement process and its constraints on localization of associated orebody: A case study in the Shizishan orefield of the Tongling Ore Cluster, east China

Hongsheng Liu, Liangming Liu, Yan Chen, Michel Faure, Xu Xia, Hongzhi Wu, Wei Cao

▶ **To cite this version:**

Hongsheng Liu, Liangming Liu, Yan Chen, Michel Faure, Xu Xia, et al.. Spatial-temporal heterogeneity of magma emplacement process and its constraints on localization of associated orebody: A case study in the Shizishan orefield of the Tongling Ore Cluster, east China. Ore Geology Reviews, 2021, 39 (Part B), pp.104587. 10.1016/j.oregeorev.2021.104587 . insu-03439459v2

HAL Id: insu-03439459

https://insu.hal.science/insu-03439459v2

Submitted on 17 Dec 2021

HAL is a multi-disciplinary open access archive for the deposit and dissemination of scientific research documents, whether they are published or not. The documents may come from teaching and research institutions in France or abroad, or from public or private research centers.

L'archive ouverte pluridisciplinaire **HAL**, est destinée au dépôt et à la diffusion de documents scientifiques de niveau recherche, publiés ou non, émanant des établissements d'enseignement et de recherche français ou étrangers, des laboratoires publics ou privés.

Distributed under a Creative Commons Attribution - NonCommercial - NoDerivatives 4.0 International License

Ore Geology Reviews 139 (2021) 104587

Contents lists available at ScienceDirect

Ore Geology Reviews

journal homepage: www.elsevier.com/locate/oregeorev

Spatial-temporal heterogeneity of magma emplacement process and its constraints on localization of associated orebody: A case study in the Shizishan orefield of the Tongling Ore Cluster, East China

Hongsheng Liu [a,b], Liangming Liu [a,b,*], Yan Chen [c], Michel Faure [c], Xu Xia [d], Hongzhi Wu [a,b], Wei Cao [a,b]

[a] School of Geosciences and Info-Physics, Central South University, Changsha 410083, China
[b] Computational Geosciences Research Centre, Central South University, Changsha 410083, China
[c] Univ. Orléans, CNRS, BRGM, ISTO, UMR 7327, F-45071 Orléans, France
[d] Tongling Nonferrous Metals Group Holdings Company, Tongling, Anhui, China

ARTICLE INFO

Keywords:
Dongguashan quartz diorite stock
Emplacement mechanism
AMS
Skarn-porphyry deposit
Tongling Ore Cluster

ABSTRACT

We present a study on the Dongguashan quartz diorite stock which is the largest Early Cretaceous intrusion associated with skarn-porphyry polymetallic ore deposit in the Tongling Ore Cluster, Middle-Lower Yangtze Metallogenic Belt in East China. The Dongguashan quartz diorite show massive texture without obvious foliation, and intrusive contact was locally observed inside of the stock. The anisotropy of magnetic susceptibility (AMS) results of the stock show two distinct groups. The Group I (G-I) is dominated by NE-SW-striking magnetic foliation with variably oriented magnetic lineation. The Group II (G-II) that intruded into G-I is characterized by steep NW-SE-striking magnetic foliation and lineation, which are parallel to the vein-like orebody developed in the stock. The 3D geometrical modelling of the stock displays a triangular shape in plan-view with an eastward bulge and irregular stock boundary in the eastern side and the contact surface is steeper in the west than that in the east, denoting that the stock was constructed with an eastward magma accretion trend. Furthermore, the Dongguashan quartz diorite has a wide range of composition and geochronological data, suggesting a multiple magma pulses emplacement model. Accordingly, we propose that the Dongguashan stock was constructed by at least two stages magma pulses. The earlier stage magma pulses intruded along the NE-SW-striking pre-emplacement structures in the country rock and partly intruded into the lithological and mechanical discontinuous interfaces which yielded the stratabound skarn orebody. The eastward magma accretion produced a highly deformed and longer heated country rock on the eastern side of the stock, favoring the orebody development along the eastern stock-country rock contact interface. The late-stage magma pulse and the parallelism among the trend of magnetic foliation of G-II, extensional structure and vein-like orebody suggest that the vein-type orebodies may controlled by both magma emplacement and regional tectonics.

1. Introduction

Study of orebody localization is a key topic for the comprehensive understanding of epithermal metallogenic systems and is indispensable for more efficient exploration of hidden deposits. Nevertheless, orebody localization is a complex geological process that has been contested for decades due to the non-linear relationship among ore-controlling factors and the development of orebodies (Reynolds, 1958; Candela, 1992; Heinrich et al., 1996; Zhao et al., 2010; Liu et al., 2011; Sun and Liu, 2014). Previous geochemical and geochronological studies have revealed that magma intrusions, which determine the type and period of ore-forming process, were the essential ore-controlling factor (e.g., Eugster, 1985; Candela, 1992; Hedenquist and Lowenstern, 1994; Thompson et al., 1999; Hua et al., 2005; Mao et al., 2008, 2011; Sillitoe, 2010; Chen et al., 2012). However, the orebody localization is strongly controlled by the physical and geological conditions of the magma emplacement process, for example, magma ascent rate, emplacement depth, accretion pattern, temperature–pressure and strain field around the intrusion (e.g., Chesley et al., 1993; Duuring and Hagemann, 2001; Candela et al., 2005; Vigneresse, 2006, 2007; Eldursi et al., 2009;

* Corresponding author at: No. 932 South Lushan Road, Changsha, Hunan Province 410083, China.
E-mail address: lmliu@csu.edu.cn (L. Liu).

https://doi.org/10.1016/j.oregeorev.2021.104587
Received 6 September 2020; Received in revised form 12 November 2021; Accepted 14 November 2021
Available online 19 November 2021
0169-1368/© 2021 The Authors. Published by Elsevier B.V. This is an open access article under the CC BY-NC-ND license (http://creativecommons.org/licenses/by-nc-nd/4.0/).

Holwell et al., 2014; Chen and Nabelek, 2017; Schöpa et al., 2017). Moreover, the geometries of pluton and pluton-country rock contact were also considered as important ore-controlling factors (Romeo et al., 2008; Liu et al., 2011, 2014; Chicharro et al., 2015; Cao et al., 2020). Hence, the reconstruction of the magma emplacement process and 3D geometry of plutons is crucial for understanding the mechanism of orebody localization.

Anisotropy of magnetic susceptibility (AMS) is a successful method to reveal the magma emplacement process, as the pattern of magnetic fabric can reflect the magma flow direction, magma accretion and regional tectonic setting (e.g., Hrouda, 1982; Ernst and Baragar, 1992; Rochette et al., 1992; Bouchez, 1997). In addition, with the development of computational modelling methods, the pluton geometry can be well defined by geophysical and borehole data (e.g., Améglio et al., 1997; Romeo et al., 2008; Liu et al., 2012; Lü et al., 2013; Sun and Liu, 2014; Wei et al., 2014). However, the application of AMS is usually impeded by limited surface exposures of the pluton, and the pluton geometry remains unclear due to the multi-use interpretation of geophysical data.

The Shizishan orefield is a representative skarn-porphyry ore deposit that is related to the Late Mesozoic intrusion and located at the center of the Tongling Ore Cluster, Middle-Lower Yangtze Metallogenic Belt, East China (rectangle inset in Figs. 1 and 2). In this study, we chose the Dongguashan quartz diorite stock as our research target (Fig. 3) as it is the largest ore-forming intrusion in the Shizishan orefield. Furthermore, the Dongguashan quartz diorite stock has been previously well studied in geochemistry, geochronology and geophysics (Xu et al., 2005, 2008, 2010; Deng et al., 2006; Xie et al., 2012; Guo et al., 2013; Wang et al., 2015; Cao et al., 2016; Liu et al., 2019). However, the localization mechanism of these randomly developed skarn-porphyry orebodies around the stock is still ambiguous. The Dongguashan quartz diorite stock has been highly explored, and mining shafts and platforms have been constructed from the surface to −850 m in the depth, so that the AMS sampling can cover the deep part of the Dongguashan quartz diorite stock. Moreover, with help of the intensive drilling projects in this area, the geometry of the stock and its related orebodies can be also reliably constructed. Therefore, through the field observation, AMS measurement, 3D geometry modeling and geochemical analysis of the stock, we acquired the distribution of magnetic fabric inside the stock, 3D geometry of the stock, as well as the variation of geochemical composition. Accordingly, we deciphered the development of the Dongguashan quartz diorite stock and the constraints on associated orebodies. Our study can help to guide the deep prospecting in the Middle-Lower Yangtze Metallogenic Belt and has implications that bear on other large-scaled intrusions.

2. Geological background

2.1. Regional geological setting

The Middle-Lower Yangtze Metallogenic Belt (Fig. 1a and b) is one of the most important Cu-Au-polymetallic belts in China, and in the world as well. It is a typical skarn-porphyry deposit belt related to Late Mesozoic intrusions developed in an intracontinental setting (Chang et al., 1991; Pan and Dong, 1999; Mao et al., 2011; Zhou et al., 2015). Hundreds of studies on these intrusions and their influences on the related skarn ore deposit had been done in the Middle-Lower Yangtze Metallogenic Belt, for examples, the geochronological, geochemical and petrological characteristics of the intrusions (e.g., Wang et al., 2004; Xie et al., 2009; Xie et al., 2018; Zhang et al., 2011; Yang et al., 2011; Yang and Lee, 2011; Wu et al., 2014), the origin of the hydrothermal fluid (e.g., Cao et al., 2012; Gu et al., 2011; Lai et al., 2007; Li et al., 2019; Zhou et al., 2000, 2007; Liu et al., 2019, 2020), and the geodynamic setting and related implications for metallogeny (e.g., Deng et al., 2011; Mao et al., 2011; Shi et al., 2013; Lü et al., 2015).

The Tongling Ore Cluster (TOC; rectangle inset in Fig. 1b and 2) is located in the center of the Middle-Lower Yangtze Metallogenic Belt, where Early Cretaceous dioritic intrusions are widely developed and

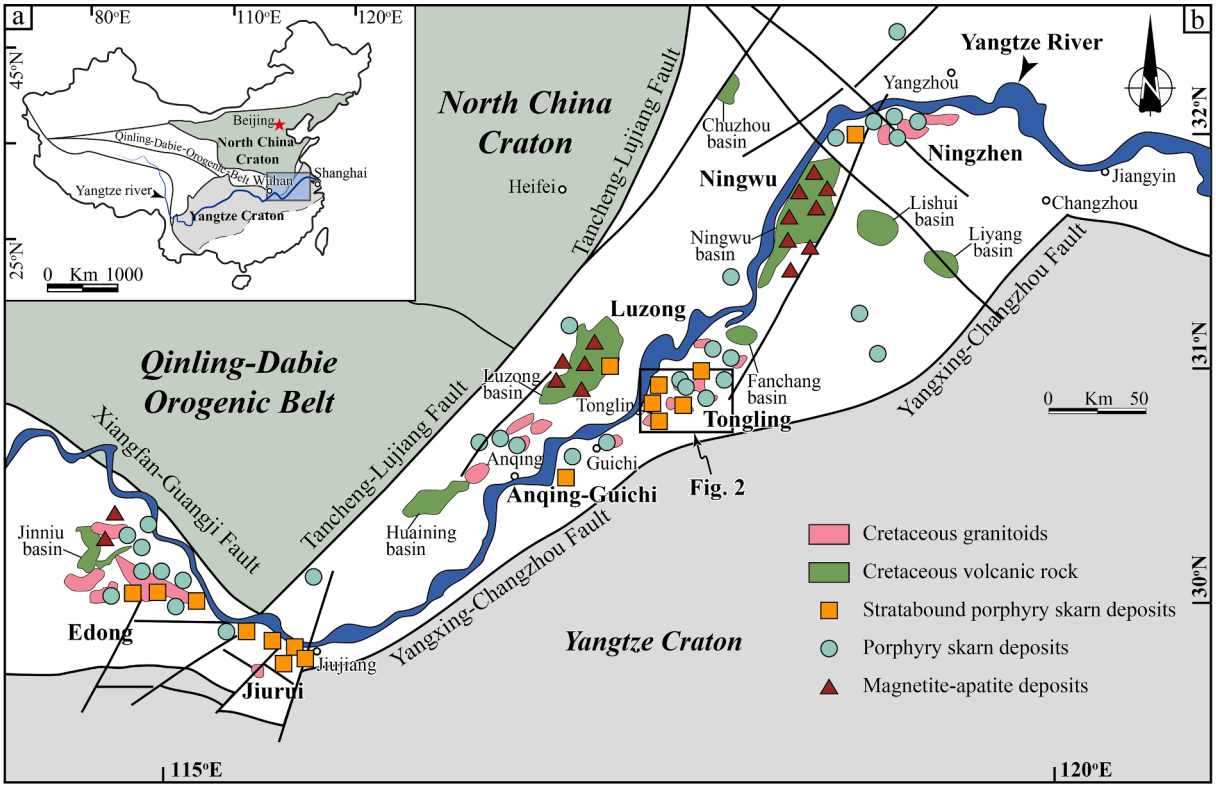

Fig. 1. (a) Tectonic sketch map of mainland China; (b) Distribution of the major Cretaceous igneous rocks and related mineral deposits in the Middle-Lower Yangtze Metallogenic Belt (modified from Pan and Dong, 1999; Mao et al., 2011).

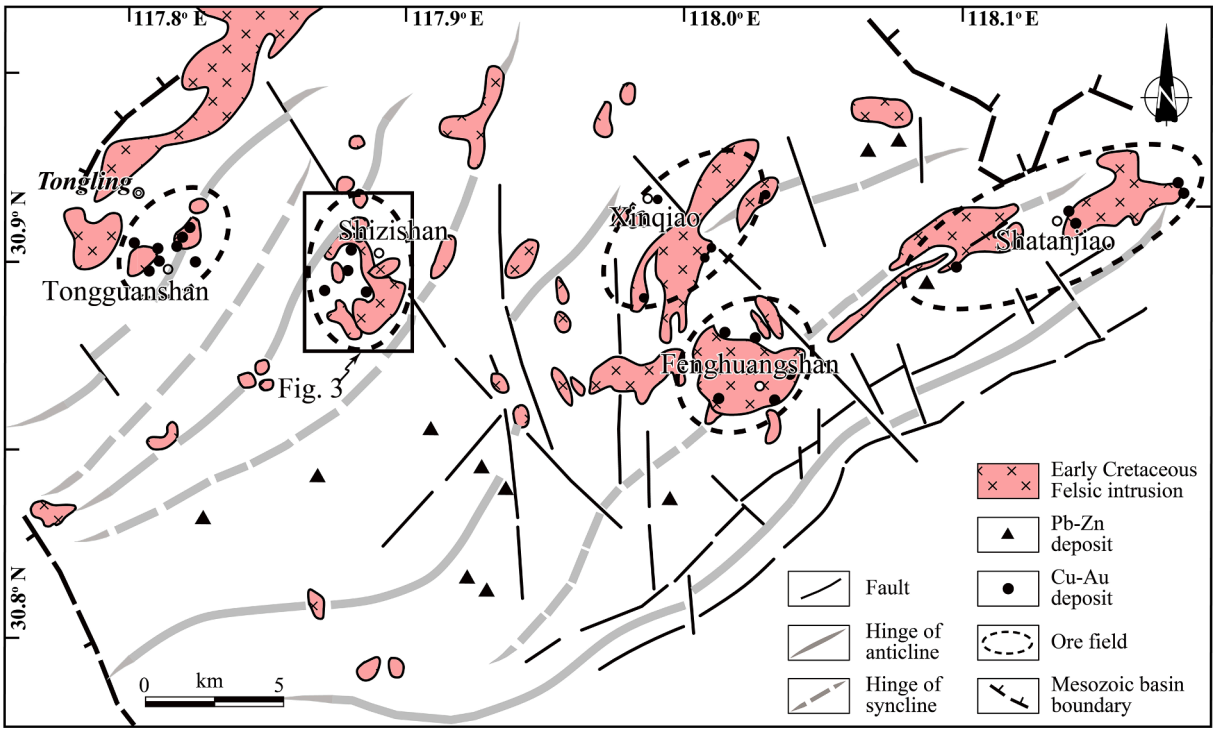

Fig. 2. Simplified magmatism-structural map of the Tongling district, Anhui province, China (The map is modified from the 1:50, 000 geological maps made by the 321 geological team in Anhui province, 1989).

often associated with skarn-porphyry Cu-Au ore deposits (Fig. 1b). The TOC consists of the Tongguanshan, Shizishan, Xinqiao, Fenghuangshan and Shatanjiao orefields (Xie et al., 2018)(Fig. 2). The stratigraphy of the TOC includes Lower Silurian to Upper Devonian siltstone, quartz-sandstone and silty shale, Middle Carboniferous to Early Triassic limestone, siliceous shale, calcareous shale and dolomite, and Late Mesozoic to Tertiary dolomitic limestone, clay shale, volcanic rocks, and continental clastic rocks (Zhai et al., 1992). Structurally, the TOC is characterized by NE-SW-striking upright folds and high-angle NW- or SE-directed thrusts, and subordinate NNE-, NNW- and NW-striking brittle faults (Fig. 2; Chang et al., 1991; Tang et al., 1998). This structural pattern is considered to be an inherited structure that represents repeated NW-SE directed compressional regional tectonic setting. In particular, this includes the Middle Triassic intracontinental subduction of South China Block under the North China Craton (Lin et al., 1985; Zhao and Coe, 1987; Mao et al., 2011), and the southwestward subduction of the Izanagi plate under the east Eurasian plate since the Late Jurassic (Sun et al., 2007; Li et al., 2011). Moreover, the NE-SW-striking Early Cretaceous Luzong and Ningwu volcanic basins and widespread Early Cretaceous intrusions and volcanism in the TOC suggest a predominantly extensional regional tectonic setting in the Early Cretaceous period (Deng et al., 2011).

2.2. The Dongguashan stock

Several Early Cretaceous intrusions are exposed in the Shizishan orefield (Fig. 3), including the Dongguashan quartz diorite (138.4 ± 1.7 Ma; Wu et al., 2013), the Baimangshan pyroxene monzodiorite (139.9 ± 1.9 Ma; Guo et al., 2013), the Jiguanshi pyroxene-quartz monzodiorite (139.8 ± 0.8 Ma; Wu et al., 2008), and the Hucun granodiorite (140 ± 2.6 Ma; Xu et al., 2008). The Dongguashan quartz diorite belongs to metaluminous and high-K, calc-alkaline-series granite (delineated by white dash line in Fig. 3; Wu et al., 2010; Liu et al., 2019). Previous geobarometric studies on the contemporary Cretaceous intrusions in this area and geophysical investigations indicate that the Dongguashan quartz diorite stock was emplaced at the brittle crust depth (ca. 4–6 km; Yangsong, 1999). The Dongguashan quartz diorite stock intruded in the hinge and eastern limb of the NE-trending Qingshanjiao anticline, which is considered as the major ore-controlling structure in the Shizishan orefield (Lu et al., 2003; Xu et al., 2005; Lü et al., 2013; Liu et al., 2014). Country rocks exposed on the surface are Middle to Lower Triassic limestone, argillaceous limestone and argillite, which were folded by the Middle to Late Triassic intracontinental orogenic event (Liu et al., 2014).

2.3. Ore deposit

With at least 10 exploited ore deposits and copper and gold reserves of more than 1.5 Mt and 20 t, respectively (Xu et al., 2014), the Shizishan orefield is economically the most important Cu-Au district in the TOC. Especially the proven copper and gold reserves of the Dongguashan ore deposit are 0.98 Mt at 1.01% and 29 t at 0.26 g/t, respectively (Liu et al., 2014; Liu et al., 2018). According to previous studies, there are three major ore localization zones around the Dongguashan stock, i.e. the Dongguashan, Datuanshan and Huashupo ores.

3. Field observation and sampling

The Dongguashan quartz diorite stock is not well exposed on the surface (Fig. 3), and fresh quartz diorite outcrops were revealed only by the ore exploration. The Dongguashan stock mainly consists of medium to fine grained quartz diorite (Fig. 4a and b) and porphyritic quartz diorite occurs locally along the stock-country rock contact (Fig. 4c). The Dongguashan quartz diorite usually displays a massive texture without macroscopic foliation, but oriented hornblende grains with sub-horizontal and outward dipping plunge are locally observed in the contact zone (Fig. 4b). Metamorphosed country rock xenoliths are observed in the stock margin (Fig. 4d and e), which resemble the "exploding xenoliths" texture observed in the shallow level intrusions (Clarke et al., 1998; de Saint-Blanquat et al., 2001). Moreover, the disharmonic folding of limestone strata (Fig. 4f) can be observed, suggesting the existence of decollement sliding in the country rocks.

The orebody developed around the Dongguashan quartz diorite stock

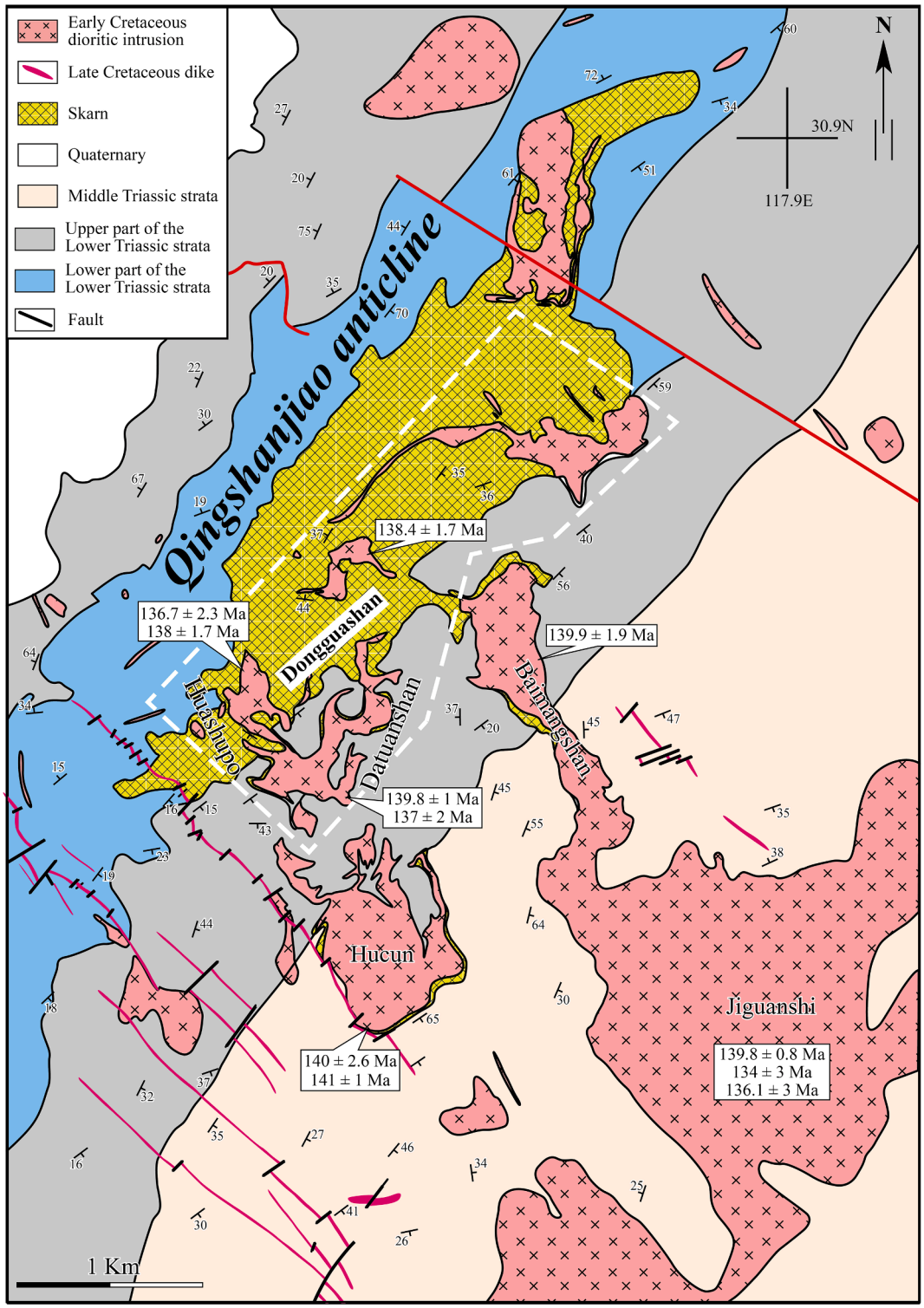

Fig. 3. Geological map of the Shizishan Orefield. The Dongguashan stock is delimited by the dashed line. The age data presented in the map are collected from Wu et al., 2008; Xie et al., 2009; Xu et al., 2008; Guo et al., 2013; Liu et al., 2019.

is characterized by stratiform (Fig. 5a), massive (Fig. 5b), veinlet and vein-like textures (Fig. 5c and d). The major sulfides are chalcopyrite, pyrite, magnetite, pyrrhotite, and the major gangue minerals are calcite and dolomite. Furthermore, our field investigation found widely developed extension related structures. For example, (1) the large-scale fracture zone developed in the stock with occurrence of 120°/66°SW (Fig. 5b), (2) the conjugated vein-type chalcopyrite ore dipping to SW and NE (ca. 0.5 to 2 cm in width; Fig. 5c and e), and (3) widely developed southwest dipping calcite veins in the stock and its country rocks (Fig. 5d and f).

According to the architecture and layout of the mine shaft and platforms in the study area, we have chosen seven mine platforms for AMS sampling, i.e. −390 m, −460 m, −580 m, −670 m, −730 m, −790 m and −850 m. A total of 41 AMS sampling sites have been collected at different depths from −390 m to −850 m, which are evenly distributed along the accessible mining channels with an interval of ca. 100 m. Due

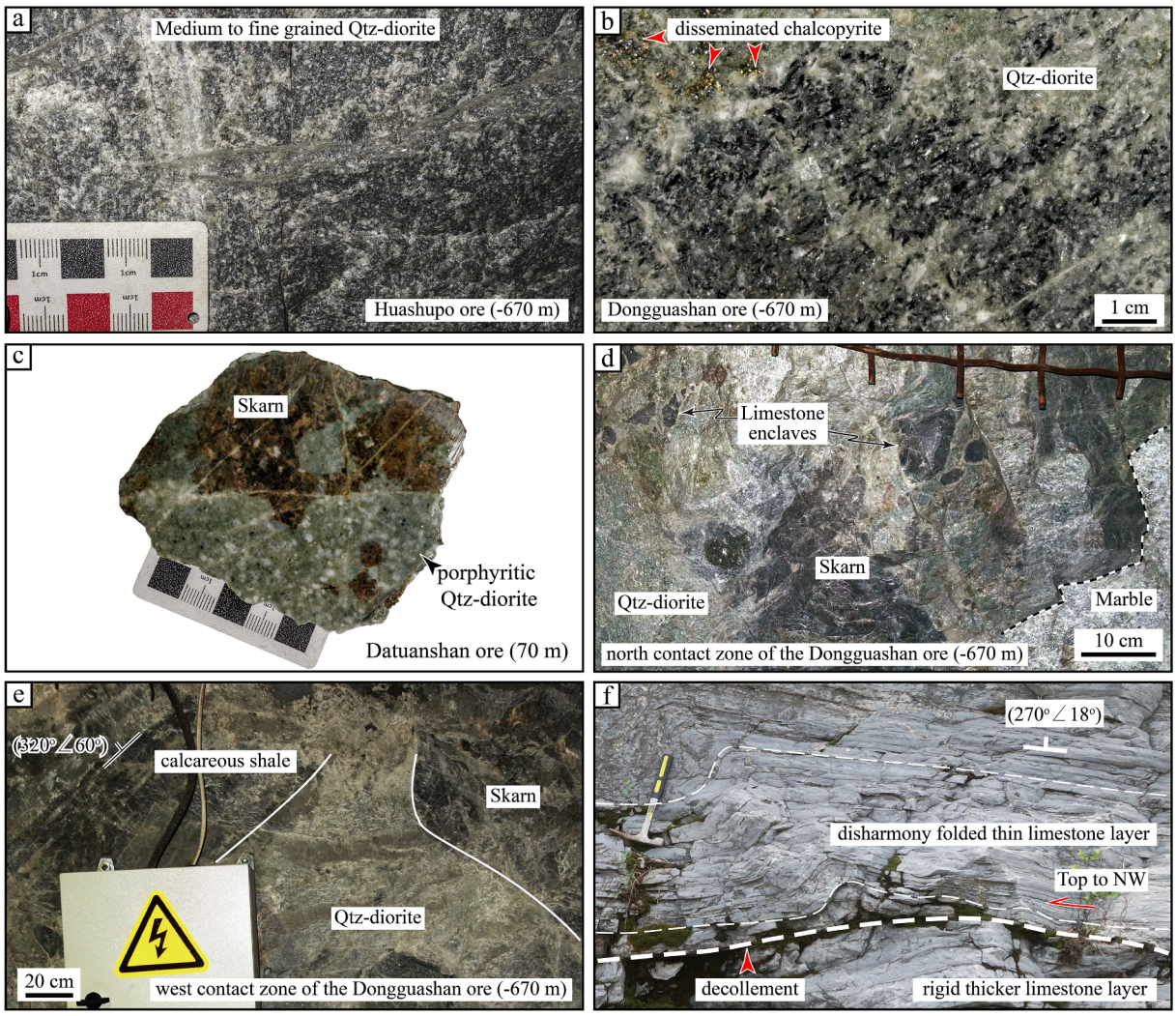

Fig. 4. (a), (b) and (c) Field observations of the Dongguashan quartz diorite stock; (d) and (e) Irregular intrusive contact and country rock xenoliths developed in the Dongguashan stock; (f), (g) and (h) Highly deformed country rocks and its deformation characters.

to the limited resolution of the GPS signal in the mining channels and short distances between different sites, the locations of AMS sampling are presented on the plan-view of the stock. The AMS samples were collected with a portable gasoline drill and oriented using a magnetic compass. The collected core samples were cut into standard cylindrical specimens, i.e. 2.2 cm in height and 2.5 cm in diameter, for AMS measurements. Detailed sampling information is listed in Table 1.

Concurrently, representative massive fresh quartz diorite samples were collected from the −670 m platform, which is the largest section of the Dongguashan stock revealed by current miming projects, for geochemical analysis in order to investigate the horizontal variation of composition inside the stock. The locations of these samples are the same as the AMS sample at this platform.

4. Analytical methods

4.1. Anisotropy of magnetic susceptibility (AMS)

The magnetic susceptibility (K) is defined as the ratio of the induced magnetization (M) to the applied field (H), while the intensity of magnetization is usually nonuniform due to the preferred orientation of minerals in the rock (Hrouda, 1982; Tarling and Hrouda, 1993), which is named as the Anisotropy of the Magnetic Susceptibility (AMS). The AMS is a second-order tensor of the magnetic susceptibility in a preferred direction, and it can be expressed by a magnetic susceptibility ellipsoid with three mutually perpendicular susceptibility axes, i.e. $K_1 \geq K_2 \geq K_3$ (Tarling and Hrouda, 1993; Borradaile and Jackson, 2004). K_1 and K_3 represent the magnetic lineation and pole to the magnetic foliation, respectively. Moreover, several parameters were calculated with the measured values of K_1, K_2 and K_3 by the program Anisoft (version 4.2, AGICO), for example, the mean bulk magnetic susceptibility ($K_m = 1/3 (K_1 + K_2 + K_3)$, the corrected degree of anisotropy ($P_J = \exp\sqrt{\{2[(\eta_1-\eta)^2+(\eta_2-\eta)^2+(\eta_3-\eta)^2]\}}$ and the shape parameter ($T=(2\eta_2-\eta_1-\eta_3)/(\eta_1-\eta_3)$), where $\eta_n = \ln K_n$ and $\eta = (\eta_1 + \eta_2 + \eta_3)/3$. Km indicates the mean bulk magnetic susceptibility of different magnetic carriers, including the ferromagnetic, paramagnetic and diamagnetic minerals, and the P_J and T values represent the eccentricity and shape of the magnetic ellipsoid, respectively (Jelínek and Kropáček, 1978; Hrouda, 1982).

The mineralogical investigations, including thermomagnetic measurement, Isothermal Remanence Magnetization (IRM) and hysteresis properties, were conducted on representative samples to reveal the contribution of different magnetic carriers to the bulk magnetic susceptibility. The thermomagnetic measurements were performed at the Paleomagnetism Laboratory of Nanjing University with the CS3 furnace coupled with a KLY-3S Kappabridge, and protective argon gas was used. The samples were heated from 50° to 700° with constant heating and cooling rate of 9°/min. The hysteresis loops and IRM measurement were carried out at the Key Laboratory of Paleomagnetism and Tectonic

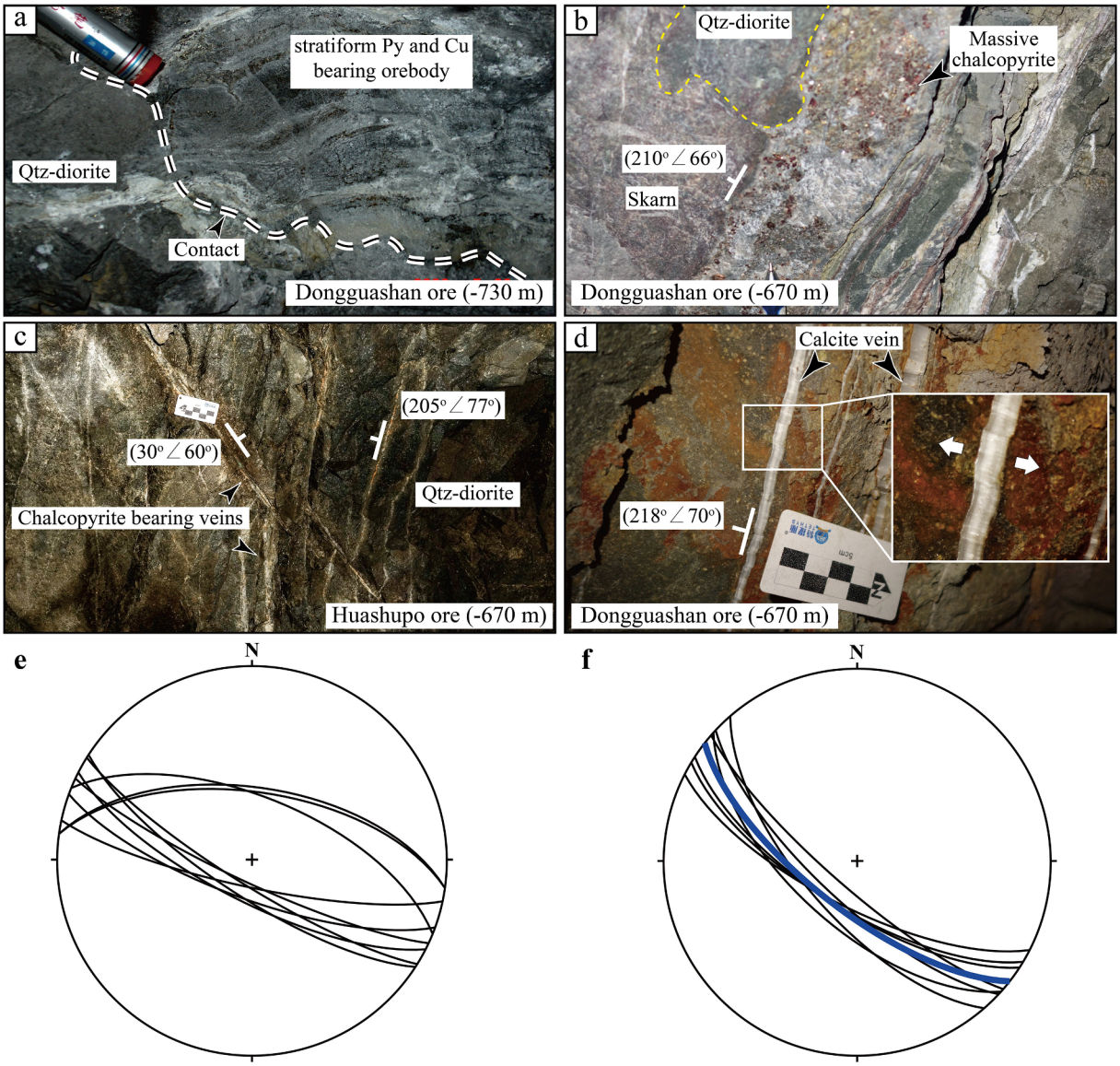

Fig. 5. (a) Restored 3D geometry of the Dongguashan stock with locations of major orebodies. (b) Stratiform orebody developed in the contact. (c) Massive chalcopyrite orebody in the stock boundary. (d) vein-type orebody inside the Dongguashan stock. (e) Southwest dipping *syn*-tectonic calcite vein in the country rocks. (f) and (g) show the lower hemisphere projection (Schmidt-Lambert projection) of conjugated ore veins and extensional fractures, respectively.

Reconstruction of Ministry of Natural Resources (Beijing). Magnetic hysteresis loops and FORCs can reveal both the grain size and domain state of magentic minerals and were obtained using a Lakeshore 8600 Vibrating Sample Magnetometer (VSM). For the magnetic hysteresis loop experiments, the powdered samples were subjected to a cycled field of ± 600 mT. A slope correction was applied to remove the impact of paramagnetic contributions.

4.2. Whole-rock major and trace element analyses

Whole-rock major and trace element analyses were conducted at the ALS Chemex Co., Ltd (Guangzhou, China). The major element concentration was determined by an X-ray fluorescence (XRF) spectrometer with an analytical precision better than ± 0.01%. Trace elements were measured using PerkinElmer ICP-MS with an analytical precision better than ± 5% for most elements. Detailed analytical methods and procedures can be found in Liang et al. (2000).

4.3. 3D geometry modelling

The 3D geometry of the Dongguashan quartz diorite stock and its related ore deposit was mainly defined by the borehole data from the Tongling Nonferrous Metals Group Holdings Company. All these data were integrated in the Micromine and GOCAD platforms, and the boundary of the geological body at shallow levels (<-850 m) without borehole data was mainly deduced by using the Micromine platform with Kriging interpolation and smoothed at the COCAD platform. Detailed approaching process is reference to Liu et al. (2012).

5. Results

5.1. Petrographic texture investigation

A total of twenty-four core specimens were selected from forty-one AMS sampling sites to prepare the oriented thin sections for petrographic texture investigation (Fig. 6a). The Dongguashan quartz diorite mainly consists of plagioclase, K-feldspar, quartz, biotite, hornblende,

Table 1
Sampling information and site-mean AMS results of the Dongguashan stock.

Site	Litho.	Depth (m)	n	Km(10^{-6}SI)	P_J	T	Site mean AMS results			
							K_1	α_{95}(max/min)	K_3	α_{95}(max/min)
							Dec (°)/Inc(°)	(°)	Dec (°)/Inc(°)	(°)
HSP01	Qtz-diorite	−390	7	5010	1.14	0.04	250.2/70.4	15.4/4.9	109.7/15.4	16.1/7.8
HSP02	Qtz-diorite	−390	5	17,700	1.20	−0.08	111/46.3	16.5/13.2	299.7/43.4	15.1/12.3
HSP03	Qtz-diorite	−390	5	6080	1.24	0.66	189.4/16.9	22.1/5.1	293/37.6	15.7/4.6
DTS04	Qtz-diorite	−390	5	5400	1.18	0.08	141.4/82.7	17.1/10.4	272.9/4.9	15.3/5
DTS05	Qtz-diorite	−390	5	662	1.02	0.03	222/56.1	22.8/11.6	106/16.4	29.6/14.2
HSP06	Qtz-diorite	−460	6	1430	1.10	0.50	209.1/60.7	25/20.2	29.9/29.3	25.4/11.4
DTS07	Qtz-diorite	−460	5	6380	1.10	−0.31	107.7/46.4	7.8/5.3	338.4/31.1	10.6/4.3
DTS08	Qtz-diorite	−460	7	17,800	1.13	0.63	267.9/36.3	19.2/6.2	1.6/5	8/3.3
DTS09	Qtz-diorite	−460	7	11,000	1.14	−0.44	186.8/81.1	16.7/8.2	326.1/6.7	21.9/9.3
DTS10	Qtz-diorite	−460	6	977	1.03	0.02	48.5/12.4	5.4/3.9	310.0/34.2	12.4/1.7
HSP11	Qtz-diorite	−580	5	2510	1.24	0.20	169.5/33.2	21.5/11.9	275.6/23	14.5/13.2
HSP12	Qtz-diorite	−580	5	16,200	1.06	0.39	227.9/23.4	11.3/7	333.2/31.2	74.5/8.7
DTS13	Qtz-diorite	−580	5	5090	1.13	−0.07	132.4/68.4	18.2/16.9	341.2/19.1	34.8/5.2
DTS14	Qtz-diorite	−580	5	1860	1.07	−0.14	67.9/2.1	9.6/4	332.7/68	15.3/3.5
DTS15	Qtz-diorite	−580	5	2050	1.12	0.22	201.1/62.1	11.5/5.1	332.3/19.2	17/4.2
HSP16	Qtz-diorite	−670	5	8240	1.12	0.53	152.1/51.8	35.5/12.8	47.4/11.3	23.1/9.5
HSP17	Qtz-diorite	−670	5	12,900	1.09	0.24	317.1/63.5	18.9/11.0	193.9/15.3	17.7/10.2
DTS18	Qtz-diorite	−670	6	4780	1.25	−0.46	137.7/72	8.1/4.1	43.3/1.4	13.7/4.9
DTS19	Qtz-diorite	−670	6	4120	1.18	0.59	135.8/17.5	51.7/13.2	44.1/5.3	26.7/17.2
DGS20	Qtz-diorite	−670	7	30,200	1.08	−0.25	122.6/40.1	25.8/8.5	17/17.7	12.5/9.9
DGS21	Qtz-diorite	−670	6	9520	1.05	0.26	236.9/3.8	36/15.8	330.9/46.4	21.1/8.6
DGS22	Qtz-diorite	−670	5	859	1.10	0.30	260.7/37.9	38.3/13.6	149.3/25.2	29.2/4.5
DGS23	Qtz-diorite	−670	5	13,900	1.10	0.08	280.5/74.3	44.6/5.1	152.8/9.8	14/5.9
HSP24	Qtz-diorite	−730	6	14,100	1.18	−0.38	120.8/37	5.1/0.8	258.8/44.6	18/4.4
HSP25	Qtz-diorite	−730	5	25,000	1.05	0.29	163.8/8.3	32.7/8.3	259.4/62.1	14.6/12.6
DTS26	Qtz-diorite	−730	6	16,000	1.12	−0.32	319.5/19.5	7.2/3.6	59.2/25.4	7/2.9
DTS27	Qtz-diorite	−730	6	3380	1.12	−0.20	168.9/8.6	13.8/5.7	76.6/14.3	10.1/8.1
DGS28	Qtz-diorite	−730	6	52,400	1.06	−0.02	216.4/15.3	21.7/4.1	324.1/48.2	10.8/2.5
DGS29	Qtz-diorite	−730	5	6000	1.15	0.40	263.5/27.2	63.5/5.9	3.3/18.3	11.2/2.8
DGS30	Qtz-diorite	−730	6	19,900	1.06	0.11	236.1/35.8	15.3/10.7	332.7/9	11.5/6.1
DGS31	Qtz-diorite	−730	5	4670	1.06	0.04	300.2/10.8	5.4/4.2	205.7/22.1	17.1/3.7
HSP32	Qtz-diorite	−790	7	3650	1.22	0.21	152.6/38.2	21.3/6.4	262.9/23.8	17.2/7.6
DGS33	Qtz-diorite	−790	5	12,100	1.10	0.14	224.6/65	7.8/4.5	132.5/1	14/4.5
DGS34	Qtz-diorite	−790	5	2380	1.05	−0.11	90.1/1.1	9.8/2.7	183.4/71.1	11.9/5.4
DGS35	Qtz-diorite	−790	5	39,000	1.12	0.24	131/6.9	26.5/10	221.3/1.9	17.3/10.4
DGS36	Qtz-diorite	−790	7	164	1.03	0.12	275.3/2.5	15.4/5.3	184.1/24.5	16/3.6
HSP37	Qtz-diorite	−850	6	14,400	1.19	0.14	144.9/74.1	12.1/8.9	46.5/2.4	16/5.2
DGS38	Qtz-diorite	−850	5	19,900	1.10	−0.04	262.8/37.6	23.5/6.0	160.9/15.1	16.0/5.8
DGS39	Qtz-diorite	−850	5	41,300	1.21	0.52	49.1/49.3	23.6/5.2	302.0/14.1	15.4/5.0
DGS40	Qtz-diorite	−850	5	171,000	1.25	0.36	184.0/45.9	47.8/12.5	74.0/18.3	13.1/4.2
DGS41	Qtz-diorite	−850	5	33,400	1.14	0.09	140.2/73.3	14.9/10.9	331.8/16.3	21.1/10.8

Note:
(1) Site: sampling site, n: number of specimen at sampling site; Km: bulk magnetic susceptibility, P_J: degree of susceptibility anisotropy, T: shape parameter of the AMS ellipsoid, K_1: Magnetic lineation, K_3: The pole of the magnetic foliation, Inc.: Inclination, Dec.: Declination, α_{95} (max/min): the long and short axes of the confidence ellipsoid at 95% level.
(2) The unfilled and light grey filled lines represent the data of the Group-I and Group-II sites, respectively.

and is associated with sphene, magnetite, pyrite, apatite and zircon (Fig. 6b-6e). Some of the Dongguashan quartz diorites display a porphyritic texture, characterized by relatively larger feldspar crystals (Fig. 6b-6e). The minerals show a euhedral to sub-euhedral habitus, and no textures related to sub-solidus high temperature deformation have been observed. Sericitization is usually developed along the cleavage of the minerals (Fig. 6b). Magnetite and pyrite are widely distributed in all the samples and are present in interstitial clots and aligned parallel to the long axis of the minerals (Fig. 6f) or in interstitial crystals (Fig. 6g).

5.2. AMS of the Dongguashan stock

5.2.1. Rock magnetic minerals

Six representative thermomagnetic measurements were performed. The heating curves show a gradual decreasing trend indicating the existence of paramagnetic minerals (Fig. 7a-7f). A moderate to slight drop at 325 ℃ for the samples collected from the depths shallower than −670 m suggests the presence of pyrrhotite (Fig. 7a-7d), and a rapid drop at 580 ℃ for all the samples is most likely due to the existence of magnetite (Fig. 7a-7f). An obvious increase of magnetic susceptibility during cooling implies that mineralogical phase transformation occurred during the thermal experiment, for instance, pyrrhotite and pyrite transformed into magnetite at ~500 °C (Dunlop and Özdemir, 1997). The shapes of the hysteresis loops of these samples are similar to that of ferromagnetic minerals (Fig. 7h-7j) with low values of magnetic coercivity (Fig. 7k–m). Moreover, the isothermal remanence measurements show similar rapid increasing and saturation trend at ca. 300 mT (Fig. 7k–m). Accordingly, the magnetic minerals in the Dongguashan quartz diorite are composed of paramagnetic minerals, e.g., biotite and feldspar, and low-coercivity ferromagnetic minerals, e.g., magnetite and pyrrhotite. The thin section observations show a relatively high volume-ratio of magnetite (Fig. 6e–6f), suggesting that the magnetite may be the major magnetic susceptibility carriers in the Dongguashan quartz diorite.

5.2.2. Magnetic parameter data

The magnetic parameters of quartz diorite in the Dongguashan stock, for instance, Km, P_J and T, are provided in Table 1, and Km vs. P_J and T vs. P_J diagrams are presented in Fig. 8. More than 90% sites show high bulk magnetic susceptibility, i.e. $K_m > 10^{-3}$SI (Fig. 8a), confirming that

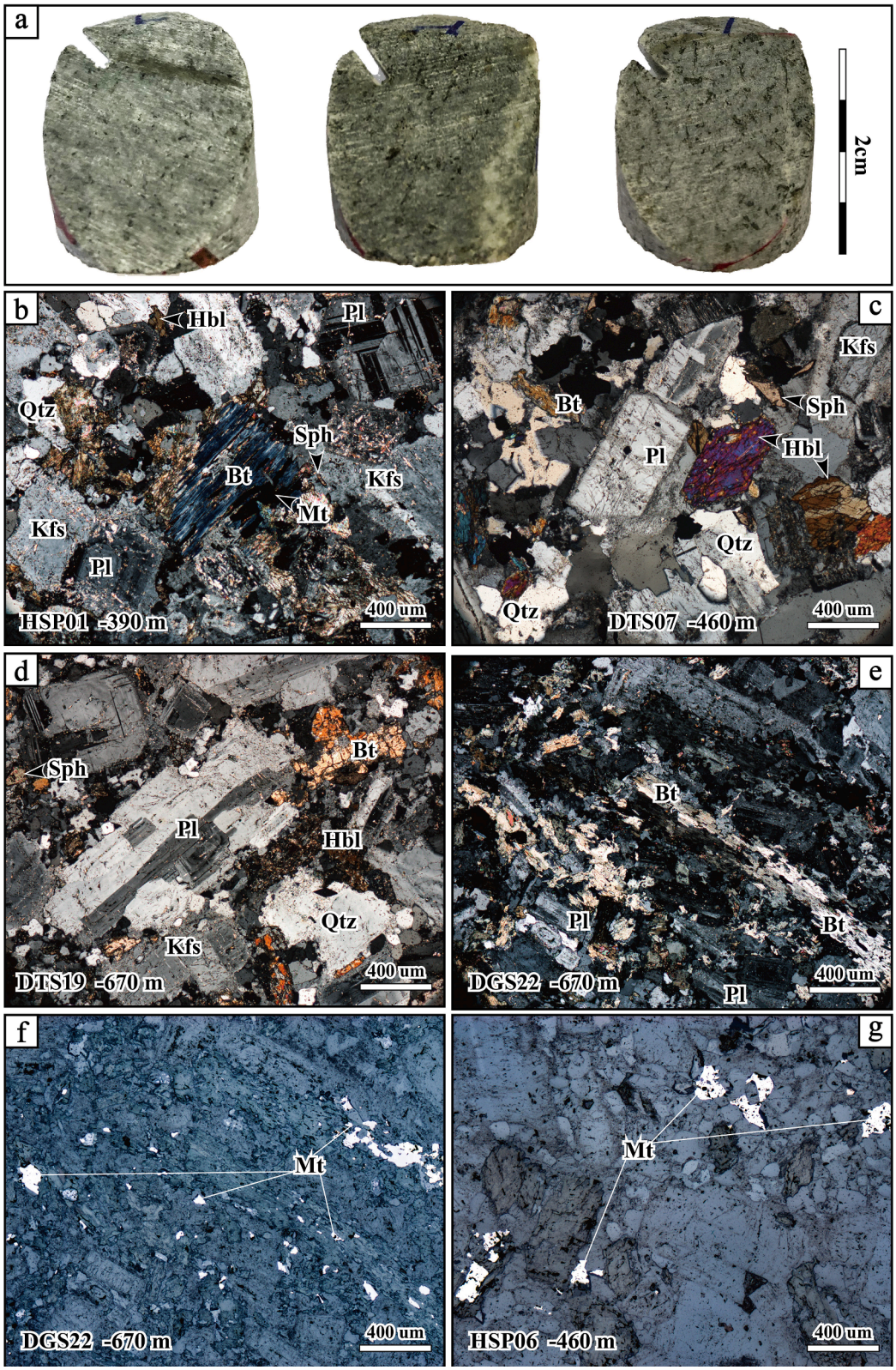

Fig. 6. (a) Cross profiles of cylinder core specimens prepared for oriented thin section. (b) to (g) Photomicrographs of thin sections of the representative quartz diorite in the Dongguashan stock. Abbreviations: Bt-Biotite, Hbl: Hornblende, Kfs: Potassium feldspar; Mt: Magnetite; Pl-Plagioclase, Qtz: Quartz; Ser: Sericite; Sph: Sphene.

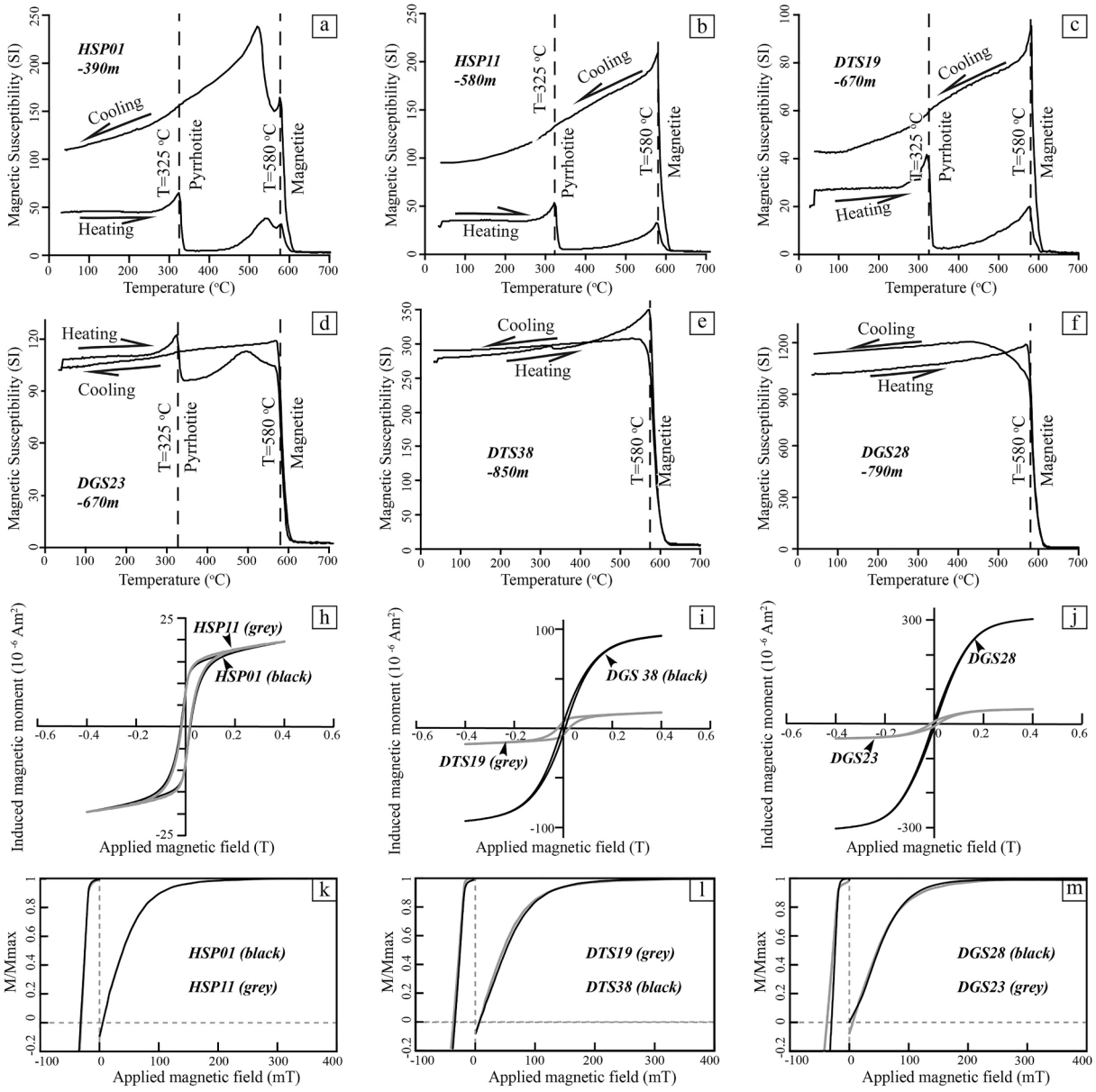

Fig. 7. Harker diagrams for variation of SiO_2 with other major elements from this and previous studies (solid grey symbols). Samples with high and low content of SiO_2 are classified into Group I and Group II, respectively. Detailed data are listed in supplementary Table S1.

these samples are dominated by the ferromagnetic minerals. Moreover, no linear correlation has been observed between the bulk magnetic susceptibility and corrected degree of anisotropy, denoting that the magnetic fabric is mainly defined by the rock composition (Borradaile, 1988). Over seventy percent of sites have corrected degree of anisotropy values lower than 1.15 (Table 1 and Fig. 8a), indicating that the magnetic fabric is mainly primary (Hrouda, 1982; Rochette et al., 1992). The sites with high P_J value are close to the stock boundary, which may be due to the intense interaction of the magma intrusion with the country rocks (Table 1 and Fig. 8). The majority of shape parameter values are positive (Table 1 and Fig. 8b), suggesting the prevalence of oblate ellipsoids, except for samples collected from the south part of the stock, which are dominated by negative values (Table 1 and Fig. 9), and thus, prolate magnetic ellipsoids are suggested.

5.2.3. Magnetic fabrics

Detailed site-mean magnetic fabrics and their positions with respect to the restored stock boundary at depth are presented in Fig. 9. Most of these sites show well developed magnetic foliations with inclinations from highly inclined dipping (40°) to vertical (89°), except for sites DTS14, HSP25 and DGS34 with gentle inclinations of ca. 20° (Table 1 and Fig. 9). According to the strike of magnetic foliation, the majority of sampling sites are characterized by NE-SW-striking and SE dipping magnetic foliation, which are labeled as Group I (G-I; white stereographs in Fig. 9). Eleven sites located in the central-southern part of the stock with depths greater than −670 m, i.e. HSP16, HSP17, DTS18, DTS19, DGS20, HSP24, HSP25, DTS26, DTS27, HSP32 and HSP37 are classified in Group II (G-II; grey stereographs in Fig. 9). The sites in G-II display relatively consistent NW-SE-striking magnetic foliations and steeper dipping angle than those in G-I (inserted stereographs in Fig. 10a and b). The magnetic lineations of G-I are characterized by highly variable plunges with directions sub-parallel or cross with the stock boundary (inserted stereograms in Fig. 10b). Especially, the sites of G-I lower than −670 m show gentle to sub-horizontal plunges of lineation (Fig. 10b). Nevertheless, the directions of magnetic lineation of G-II show a consistent NW-SE trending and variable plunges (Fig. 10c and d).

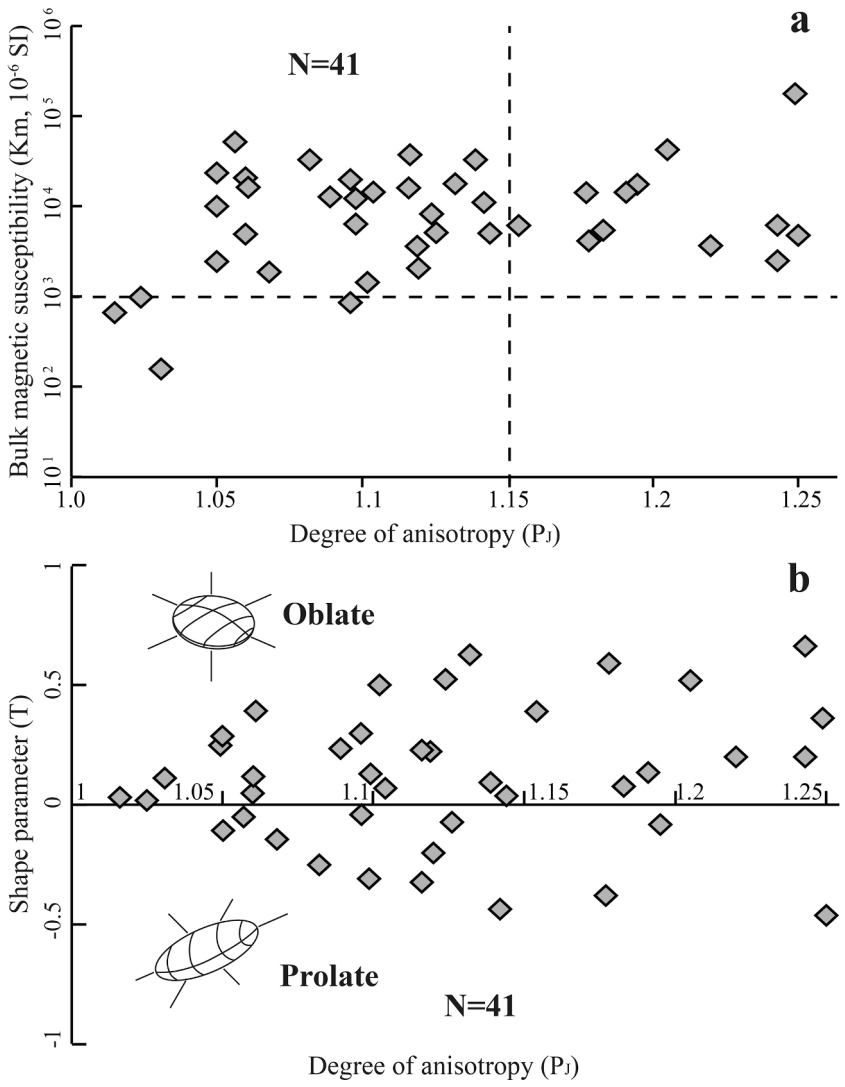

Fig. 8. Results of magnetic mineralogy analysis of representative quartz diorite samples from the Dongguashan stock. (a-f) thermal magnetic curves; (h-i) hysteresis loops, corrected for the paramagnetic linear trend; (k-m) isothermal remnant magnetization acquisition curves and backfield applications.

5.3. Whole-rock major and trace elements geochemistry

Six fresh and representative samples for geochemical analysis were collected at the −670 m platform and sampling locations are the same as the AMS sampling (Fig. 11a). The acquired geochemical data and previous geochemical analysis are presented in Table S1. Previous geochemical results of the Dongguashan stock are also included in Table S1 for a comprehensive and comparative analysis (Wang et al., 2003, 2015, Huang et al., 2004; Guo et al., 2013; Liu et al., 2019).

According to the SiO_2 content, the analyzed Dongguashan quartz diorites and previous geochemical analysis present a wide range of SiO_2 (56.5% to 65.32 wt%) and the relatively low SiO_2 content Group II (G-II: 56.48–60 wt%; Table S1 and Fig. 11). Moreover, G-I has a wider range of SiO_2 content than that of G-II (Fig. 11b-h). The TiO_2, Al_2O_3, CaO, MgO, Na_2O and P_2O_5 display steadily decrease or constant trend with increasing SiO_2, suggesting that the minor compatible behavior (Fig. 11b–g). K_2O shows constant or slightly increase in G-I with increasing SiO_2 (Fig. 11h), which may be due to the hydrothermal alteration during the subsequent mineralization process.

5.4. The 3D geometry of the stock and its related orebody

The horizontal drilling sections and 3D geometry model of the Dongguashan quartz diorite stock and related orebodies (Fig. 12) highlight several major features of the Dongguashan quartz diorite stock. The stock has a complicated shape with a principal NE-SW extending long axis. Many apophyses are formed within the strata bedding (Fig. 12b, c and d) and the skarn orebodies are mainly developed in the northern hinge and eastern limb of the Qingshanjiao anticline. The largest ore, i.e. the Dongguashan ore, was yield between the Middle to Upper Carboniferous carbonates and Upper Devonian sandstone with depth ranging from ca. −650 m to −850 m (Fig. 12a), and the other two ore deposits, i.e. the Huashupo and Datuanshan ore deposits, are localized along the contact zones of the Dongguashan stock (Fig. 12).

6. Discussion

6.1. Significance of the petrofabric investigation

The nature of the fabrics, i.e. whether primary or not, is pivotal for the interpretation. Our microscopic petrographic investigations on the Dongguashan quartz diorite and its country rocks show that the quartz diorite samples exhibit a typical magmatic texture, and intrusion-related ductile deformation was absent in the contact zone (Fig. 6). The dominantly low P_J values of the quartz diorite samples also suggest that the stock has not been significantly affected by a subsequent regional

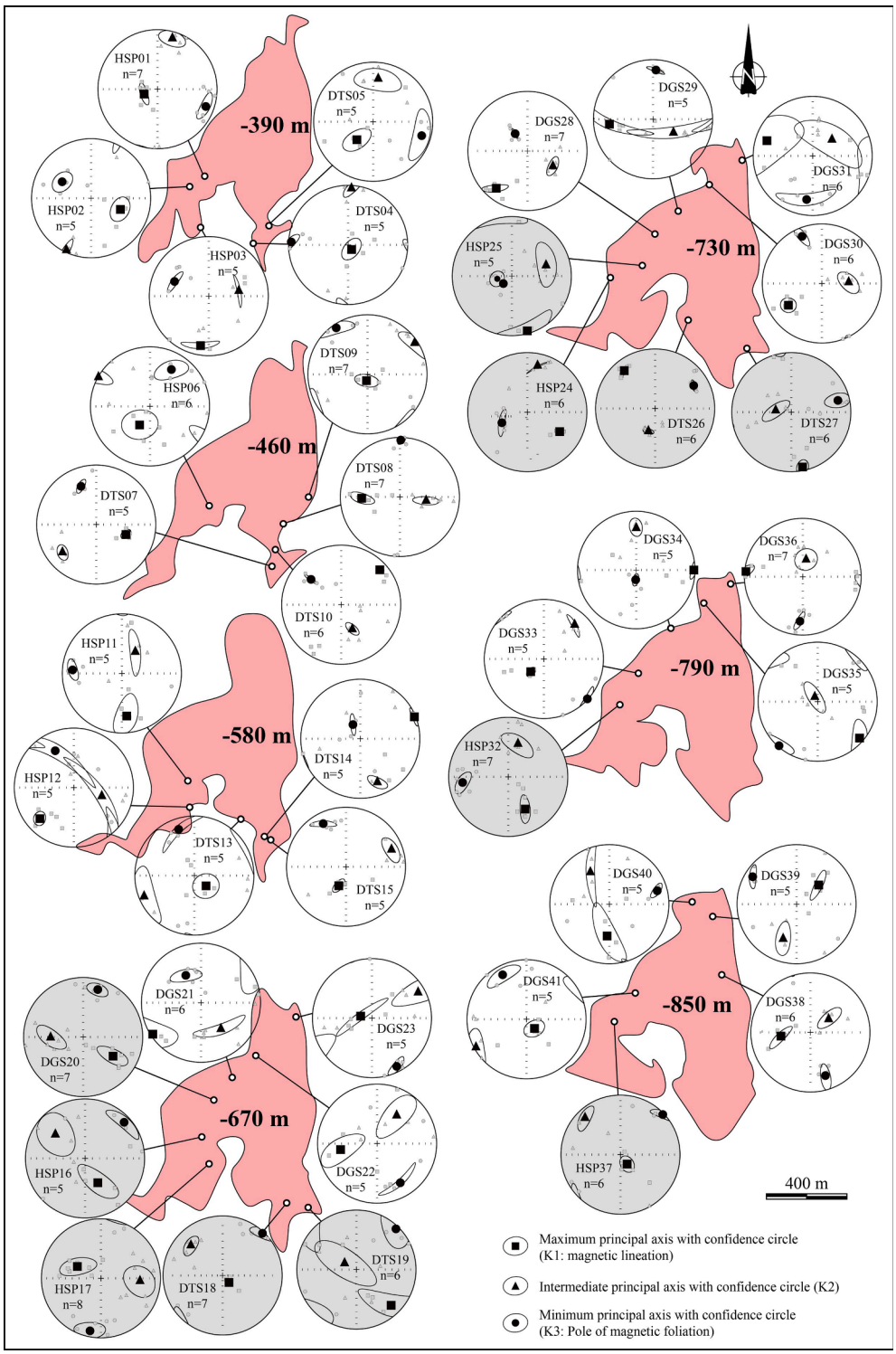

Fig. 9. Correlation of the magnetic parameters. a) K_m vs. P_J and b) T vs. P_J.

tectonic event (Hrouda and Lanza, 1989; Rochette et al., 1992). The ductile deformation of the country rock of the Dongguashan quartz diorite stock is apparent in folding and thrusting (Fig. 4f) that are considered to be inherited structures resulting from the Triassic intra-continental event instead of resulted from magma emplacement (Deng et al., 2011; Mao et al., 2011; Wang et al., 2011).

Moreover, our magnetic mineralogical analyses suggest that major magnetic carriers of the Dongguashan quartz diorite are ferromagnetic and paramagnetic minerals. According to the microscopic observations, the arrangement of the magnetite and pyrrhotite is usually parallel to the long axis of the plagioclase and/or biotite (Fig. 6e and 6f), indicating that the magnetic fabric ellipsoid is parallel to the principal finite strain axes inferred from the petrographic fabric. Namely, the K1 and K3 magnetic axes correspond to the mineral lineation and the foliation pole, respectively. Consequently, we argue that the magnetic fabrics of the Dongguashan quartz diorite revealed by our AMS investigation were primary fabric, which can be used to reveal the magma emplacement process.

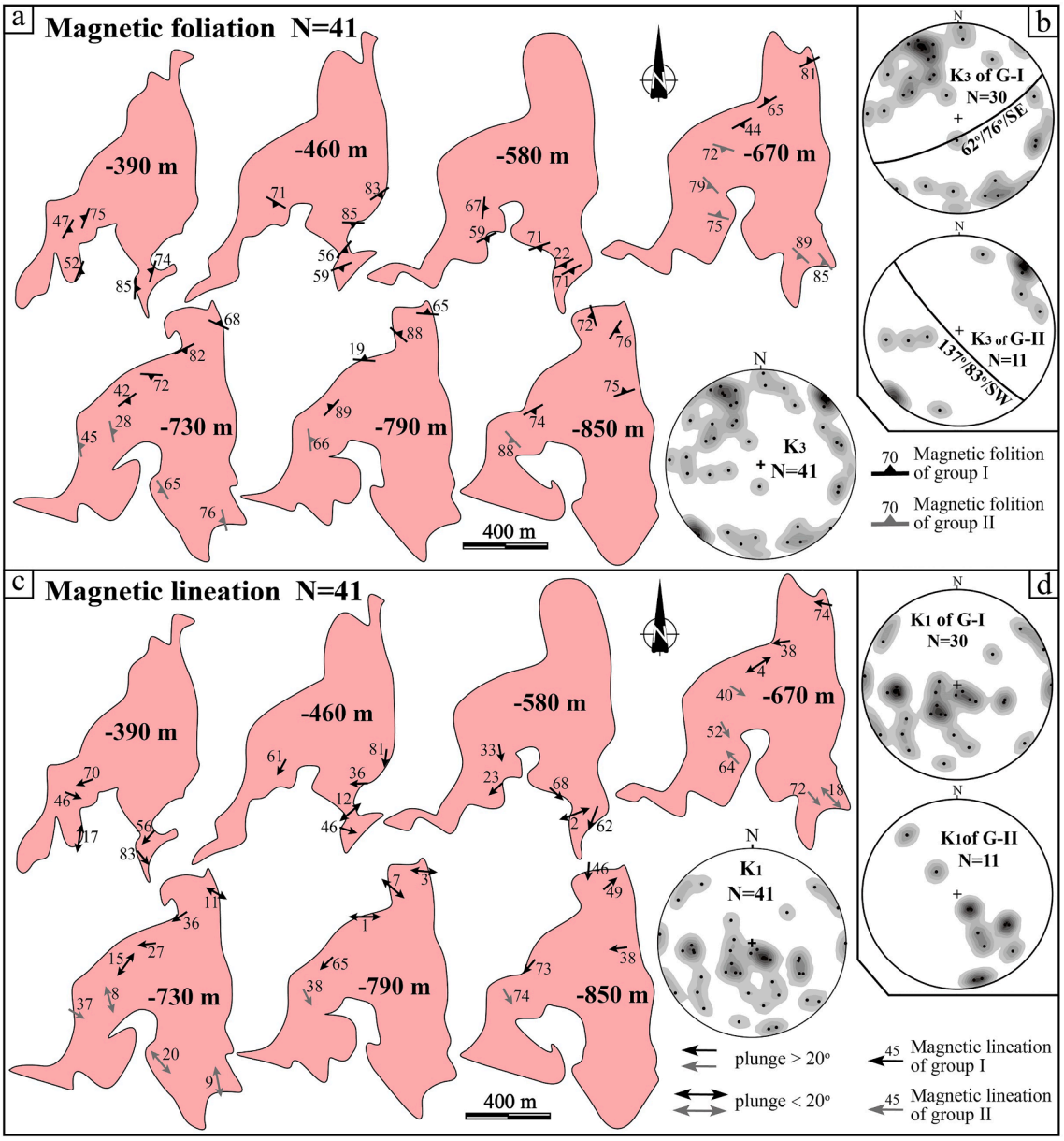

Fig. 10. Detailed AMS results of the Dongguashan quartz diorite. The white and grey stereograms are for Group I and Group II, respectively.

6.2. *Interpretation of AMS results of the Dongguashan stock*

As mentioned above, the most remarkable feature of the AMS results of the Dongguashan quartz diorite is the coexistence of two nearly orthogonal magnetic fabric groups, i.e. G-I and G-II. Thus understanding of the magnetic fabric of the Dongguashan quartz diorite stock is essential for the re-construction of the magma emplacement process. The 3D geometry modelling of the Dongguashan quartz diorite stock (Fig. 12) and a previous geobarometric study indicate that the stock has a small volume and shallow emplacement depth (ca. 4–6 km; Du et al., 2004). Therefore, we consider that the Dongguashan stock should be a rapidly emplaced and cooled stock, in terms of previous studies on the duration of pluton construction (Matzel et al., 2006; de Saint Blanquat et al., 2011). Consequently, this distinct magnetic fabric pattern cannot be produced by magma convection in the magma chamber at emplacement crust level, and detailed discussion of the AMS result is described below.

6.2.1. *AMS results for Group I*

Seventy-eight percent of the magnetic foliation of G-I is characterized by a NE-SW strike with steep or high-angle southeastward dip (Fig. 10 and Table 1). This pattern of relatively consistent strike and dip of the magnetic foliation in the Dongguashan quartz diorite stock is different from previous AMS studies on other stocks around the world, which usually present a circular array of inward dipping magnetic foliations with strike parallel to the stock boundary (Cogné and Perroud, 1988; Hrouda and Lanza, 1989; Romeo et al., 2008; He et al., 2009; Pina et al., 2010). Whereas the trend and plunge of magnetic lineation of these sites are highly variable (Fig. 10c and 10d), which is a typical feature for the fabric developed in a stock (Cogné and Perroud, 1988; Hrouda and Lanza, 1989; de Saint-Blanquat, et al., 2001). This specific magnetic fabric pattern might be produced by the NW-SE directed regional shortening setting or be affected by the pre-emplacement NE-SW-striking structures in the country rocks. Nevertheless, previous studies suggest that the Tongling Ore Cluster is mainly under extensional regime during the magma emplacement epoch (e.g., Mao et al., 2003; Li et al., 2014). The petrographic investigations on the stock and its

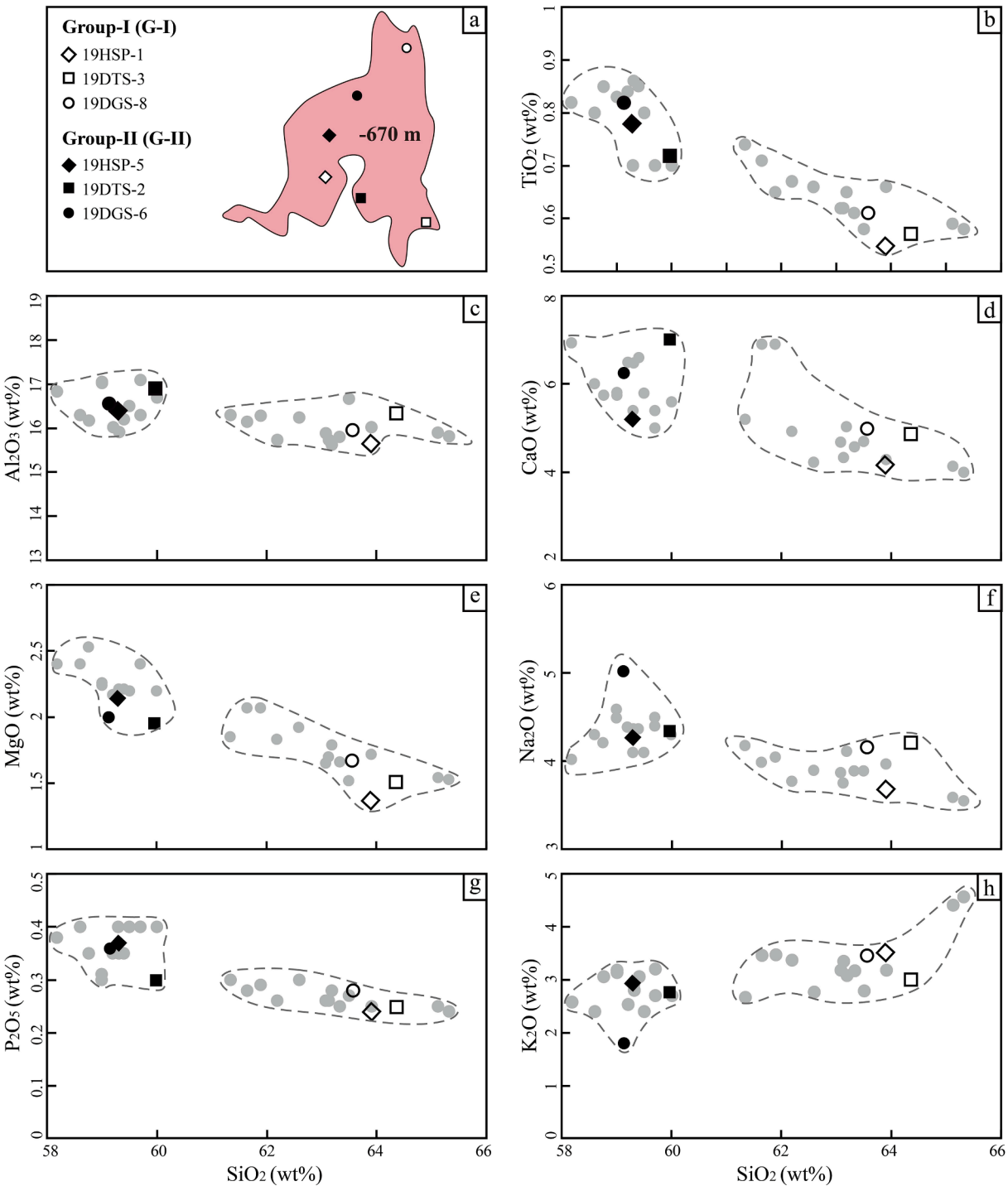

Fig. 11. (a) Magnetic foliation of the Dongguashan stock and stereogram of foliation poles, (b) Stereograms of poles of magnetic foliation for samples in Group I and Group II, respectively. (c) Magnetic lineation of the Dongguashan stock with inserted stereogram. (d) Stereograms of magnetic lineation for samples in Group I and Group II. All the projections are equal area and lower-hemisphere.

country rocks also suggest that the Dongguashan stock was not significantly influenced by any *syn*-magmatism and post-solidus regional tectonics. Hence, these evidence seem to be inconsistent with the first possibility. Alternatively, considering the parallelism between the pre-emplacement fold and fault system developed in the country rocks and the NE-SW-striking magnetic foliation, we propose that these pre-emplacement structures may serve as magma ascent paths to form the NE-SW trending steep magnetic foliations, thus the magma ascent was principally driven by its buoyancy (Marsh, 1982; Clarke et al., 1998; Paterson and TKF, 1993).

In particular, there are seven sites located at depths of −730 m, −790 m, and −850 m of G-I show the strike of magnetic foliation crosscutting the stock boundary with mainly sub-vertical to northward dip (Fig. 10a). The magnetic lineation is mainly trending NE-SW or E-W with sub-horizontal plunges. This phenomenon may be due to the boundary effect, complex magma flow or magma outflow (e.g., Ferré et al., 2002; Kratinová et al., 2006). The borehole data also confirms that the Dongguashan quartz diorite intrusion was intruded into the stratigraphic interface at these depths (Fig. 12; Liu et al., 2014).

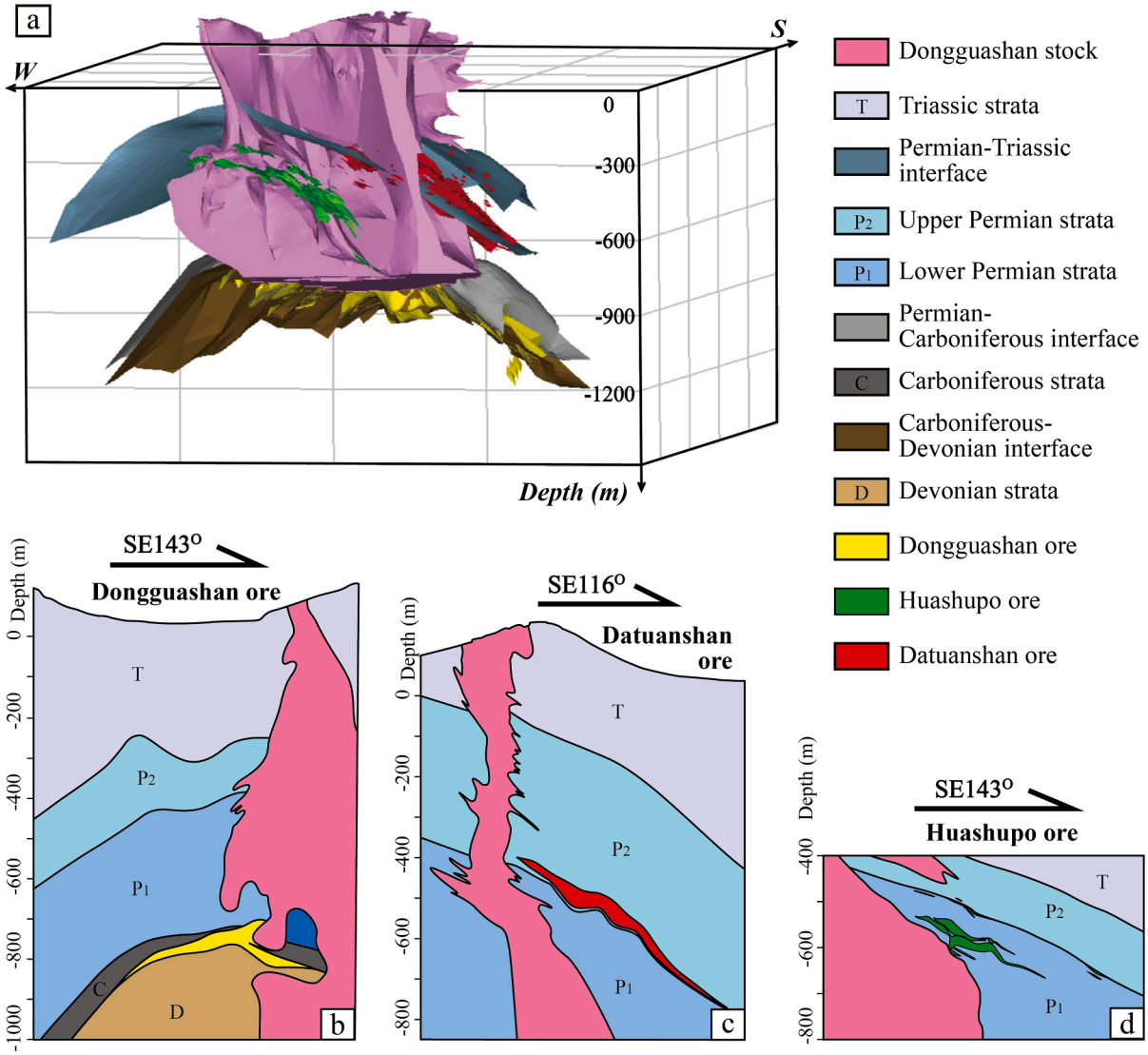

Fig. 12. (a) 3D geometric model of the Dongguashan quartz diorite stock and its related ore deposits, (b), (c) and (d) Representative drilling profiles of the Dongguashan, Datuanshan and Huashupo ore, respectively.

6.2.2. AMS results for Group II

The magnetic fabric of G-II is characterized by consistent NW-SE-striking magnetic foliation and lineation, and this preferred orientation is roughly perpendicular to those of G-I and the NE-SW-striking regional structures. In addition, we have observed pervasively developed NW-SE striking fractures, calcite veins and vein-type orebodies in the Dongguashan stock and its country rocks (Fig. 5), which are parallel to the strike of the magnetic fabric of G-II. The NW-SE oriented magnetic fabrics, fractures and veins may be produced either by regional shortening in NW-SE direction, or the magma was intruded into the NW-SE striking brittle structures, which produced by the overall extension of the upper crust in the Early Cretaceous epoch. However, contemporaneous Early Cretaceous magmatism is widely developed in the TOC, which is usually display a high-k and calc-alkaline affinity and considered to be a consequence of the regional extension (Wang et al., 2003; Wu et al., 2010; Guo et al., 2013; Zhou et al., 2015). Therefore, the hypothesis of the regional shortening is not preferred, we thus propose that the G-II magma emplacement was affected by overall extension of the upper crust.

6.3. Overview of research and tentative magma emplacement model proposal

Apart from the difference in the AMS results, a sharp intrusive contact was observed at −670 m platform (Fig. 13), suggesting that the Dongguashan was constructed by multiple magma pulses. In addition, this and previous geochemical studies on the Dongguashan quartz diorite stock show that the major elements have a wide composition range (Fig. 11 and Table S1), which may result from fractional crystallization or multiple magma pulses emplacement model. Although the major elements seem to be distributed along a regression line, whereas the higher SiO_2 content samples were collected from the outer and deeper parts of the stock compared with the less silica-rich samples (Fig. 11). This distribution opposes the normal fractional crystallization trend in a gradual cooling magma chamber (Tindle and Pearce, 1981; McNulty et al., 2000; Coleman et al., 2004). Gradual petrological change or composition zoning related to fractional crystallization is also absent in the stock. Therefore, the fractional crystallization process seems not suitable to explain the composition variation of the Dongguashan stock. Furthermore, previous geochronological studies in the Shizishan ore-field also present a wide age spectrum, indicating a relatively long time magma emplacement process (Wu et al., 2010; Yang and Lee, 2011; Guo

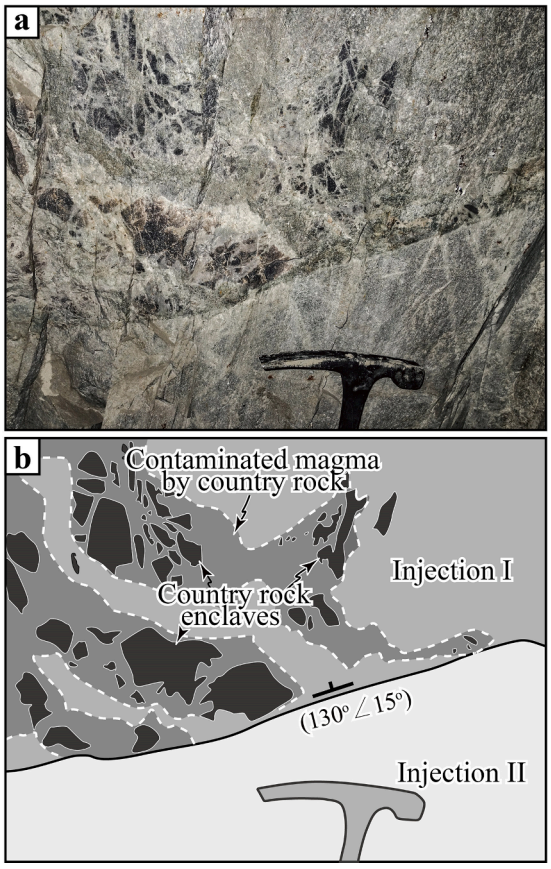

Fig. 13. (a) Photograph and (b) sketch of intrusive contact in the Dongguashan stock.

et al., 2013; Wang et al., 2015; Liu et al., 2019). In summary, all these evidence suggest that the Dongguashan quartz diorite stock was constructed by multiple magma pulses, and a two-stage magma emplacement model is proposed for the Dongguashan quartz diorite stock as described below.

On account of the samples of G-I are located in the outer part of the stock from −850 m to −390 m, and the samples of G-II are collected in the inner part of the stock with depths lower than −650 m. Moreover, the strike of magnetic foliation of G-I is cut by the G-II (Fig. 10). Therefore, we suggest that G-I and G-II belongs to the earlier and late magma pulses emplacement stages, respectively.

First, the initial magma emplacement occurred when the internal buoyancy force of the deeply seated magma chamber exceeded the lithostatic pressure of the country rocks (Fig. 14a; van der Molen and Paterson, 1979; Bachmann and Bergantz, 2004; Vigneresse, 2007). Previous studies suggest the existence of NE-SW-striking basement faults in the crust, and the upper crust was deformed by Triassic pre-emplacement regional tectonics (Deng et al., 2006), which yielded paths or channels for the magma ascent (Fig. 14a). The decollement of country rocks produced part of the space for magma emplacement (Fig. 4f). Moreover, the abundance of xenoliths observed in the stock boundary suggests that the space for magma emplacement was partly created by magma stoping (Marsh, 1982; Clark et al., 1998). The relatively more regular stock boundary in the western side of the stock than in the eastern one suggests an eastward magma accretion trend. The dilation (possibly controlled by hydrothermal fluids), inflation and uplifting of the brittle country rocks accommodated the gradual emplacement of magma (Fig. 14b).

Second, the consistent NW-SE-striking magnetic foliation of Group II samples and its parallelism with the NW-SE-striking fractures developed in the stock and country rocks, which produced by the regional extension, suggest that the emplacement of the late magma pulse was strongly controlled by these fractures (Fig. 14c).

6.4. Implications for the associated orebody localization

Our study reveals that the Dongguashan stock was constructed by at least two magma pulses. Discontinuous magma emplacement changes the temperature field, fluid composition, oxygen fugacity and elements partition coefficients, and therefore is an important mechanism for the formation of huge intrusion related ore deposits (e.g., Holzheid and Lodders, 2001; Vigneresse, 2007; Huber et al., 2012; Chelle-Michou et al., 2015).

According to the restored 3D stock and orebody geometry model, the

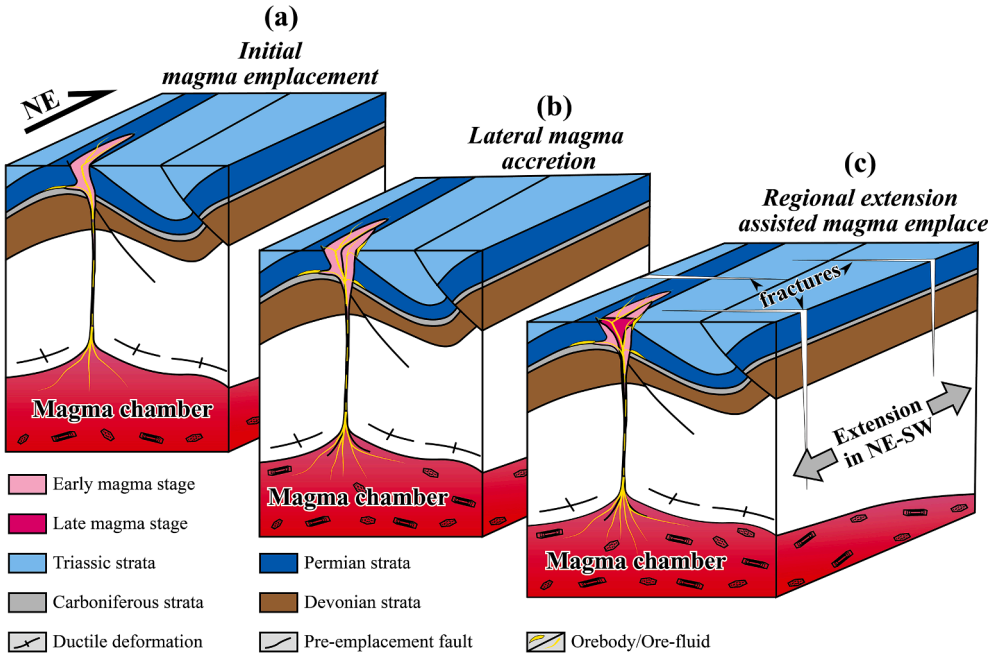

Fig. 14. Cartoon of the magma emplacement mechanism of the Dongguashan stock.

largest ore reserves are located at the Devonian-Carboniferous (D-C) stratigraphic interface with depth between ca. −650 and −950 m (Fig. 12). The occurrence of these stratiform orebodies is consistent with the flanks of the Qingshanjiao anticline, denoting that the hydrothermal fluid was intruded along the strata interface (Tang et al., 1998). The AMS results of the sites close to the stock boundary at depths of −670 to −850 m suggest that magma outflow occurred within these strata, which is also supported by tiny and rootless granitic body revealed by borehole data (Fig. 12). Previous geochemical studies also suggest that the magma is the dominant source of ore-forming fluid. Thus, the stratiform skarn orebodies were mainly yielded by the early emplaced magma pulse, which was emplaced along pre-emplacement structures or discontinuous mechanical interfaces in the country rocks.

The second orebody localization zone concerns the contact zone between the stock and country rock. This includes the Huashupo and Datuanshan skarn-type orebodies, which are developed at the eastern side of the stock at depths of −300 to −600 m, and thus are related to the earlier emplaced magma pulse (Fig. 12). According to our study, the Dongguashan stock was constructed by successive magma pulses with an eastward accretion trend and forceful-like emplacement behavior. Thus, the country rock in the eastern side of the stock has a higher degree of deformation, intense fracturing and higher permeability and temperature, which were produced by the repeated magma intrusion. In addition, the restored 3D geometrical model shows that the occurrence of the orebody in the eastern side of the stock is roughly parallel to the stock-country rock contact surface, which dips gently outward in contrast to a sub-vertical contact in the western side (Fig. 12). Consequently, we propose that different interaction between the magma and country rock may affect the localization of the orebodies.

The third type of orebody, i.e. the vein-like and veinlet-disseminated orebodies, is widely developed inside the Dongguashan stock and partly developed in the NW-SE-striking fractures (Fig. 5c and 5d). The parallelism among the ore veins, the strike of magnetic foliation of G-II and the fractures (Figs. 5 and 12) suggests that the space for the vein-like orebody was controlled by the later magma pulse.

7. Conclusions

According to our macro- and microscopic observations, geochemical and AMS analyses and 3D geometrical modelling of the Dongguashan stock, we concluded that:

1) The Dongguashan stock was constructed by at least two stages magma emplacement. The AMS results of these two magma stages can also be divided into two groups, i.e. G-I and G-II, corresponding to earlier and later magma pulses, respectively. G-I is dominated by a NE-SW striking magnetic foliation, which is parallel to the trend of the pre-empalcement folds and faults, suggesting that the magma emplacement was probably affected by the pre-emplacement structure. G-II is characterized by a NW-SE-striking magnetic foliation, which is parallel to the regional extensional structures, suggesting the control of regional extension on magma emplacement.

2) The 3D geometrical modelling of the stock presents a triangular shape with irregular and bulged boundary in the eastern side of the stock, denoting that the stock was constructed by an eastward magma accretion.

3) The AMS results suggest that the magma was intruded into the strata interface at depths between −670 to −850 m, which is the essential factor for the formation of the stratiform ore deposit in the Dongguashan area. Moreover, the eastward magma accretion resulting in highly fractured and more permeable country rocks in the eastern stock contact zone that can explain why the skarn orebodies are localized in the eastern stock contact zone. The NW-SE-striking ore veins were likely controlled by the emplacement of the late magma pulse under an extensional regional tectonic setting.

Declaration of Competing Interest

The authors declare that they have no known competing financial interests or personal relationships that could have appeared to influence the work reported in this paper.

Acknowledgements

We thank Mr. Wangsheng Jiang, Hui Jin, Yong Jiang (Tongling Nonferrous Metals Group Holdings Company) for their help in sample collection. Our thanks also go to Mrs. Xinxin Sun for her help in magnetic mineralogical analysis, and Jeffrey M. Dick for language editing. Moreover, detailed language editing and constructive suggestions on the first manuscript version from the associate editor Prof. Deru Xu was highly appreciated. We also appreciate the pertinent comments and constructive suggestions provided by Dr. Wei Wei and another two anonymous reviewers that have significantly improved the presentation of this study. Access to the Dongguashan mine and offering of borehole data by the Tongling Nonferrous Metals Group Holdings Company are highly appreciated. We also appreciate financial support from the National Natural Science Foundation of China (41372338, 41772351 and 41902209) and Research foundation of Hunan Province (2019JJ50832), French LABEX VOLTAIRE (ANR-10-LABX-100-01) and EQUIPEX PLANET (ANR-11-EQPX-0036).

Appendix A. Supplementary data

Supplementary data to this article can be found online at https://doi.org/10.1016/j.oregeorev.2021.104587.

References

Améglio, L., Vigneresse, J.L., Bouchez, J.L., 1997. Granite Pluton Geometry and Emplacement Mode Inferred from Combined Fabric and Gravity Data. In: J.L. Bouchez, D.H.W. Hutton, W.E. Stephens (Editors), Granite: From Segregation of Melt to Emplacement Fabrics. Springer Netherlands, Dordrecht, pp. 199-214. https://doi.org/10.1007/978-94-017-1717-5_13.

Bachmann, O., Bergantz, G.W., 2004. On the origin of crystal-poor rhyolites: extracted from batholithic crystal mushes. J. Petrol. 45 (8), 1565–1582. https://doi.org/10.1093/petrology/egh019.

Borradaile, G.J., 1988. Magnetic susceptibility, petrofabrics and strain. Tectonophysics 156 (1-2), 1–20. https://doi.org/10.1016/0040-1951(88)90279-X.

Borradaile G.J., Jackson M. Anisotropy of magnetic susceptibility (AMS): magnetic petrofabrics of deformed rocks. In: In: Martín-Hernández, F., Lüneburg, C.M., Aubourg, C., Jackson, M. (Eds.), Magnetic Fabric: Methods and Applications, 2004. vol. 238. Geological Society, London, Special Publications, pp. 299–360.

Bouchez, J.L., 1997. Granite is Never Isotropic: An Introduction to AMS Studies of Granitic Rocks. In: Bouchez JL, Hutton DHW, Stephens WE, editors. Granite: From Segregation of Melt to Emplacement Fabrics. Dordrecht: Springer Netherlands. p. 95–112. https://doi.org/10.1007/978-94-017-1717-5_6.

Candela, P.A., 1992. Controls on ore metal ratios in granite-related ore systems: an experimental and computational approach. Transactions of the Royal Society of Edinburgh: Earth Sciences 83 (1–2).

Candela, P.A., Piccoli, P.M., Hedenquist, J.W., Thompson, J.F.H., Goldfarb, R.J., Richards, J.P., 2005. Magmatic processes in the development of porphyry-type ore systems. One Hundredth Anniv. Vol.: Soc. Econ. Geol. https://doi.org/10.5382/av100.03.

Cao, W., Liu, L., Liu, H., Lai, F., 2020. Investigating the irregular localization of skarn orebodies by computational modeling in the Fenghuangshan Ore Field, Tongling District, Anhui Province, China. Nat. Resour. Res. 29 (5), 2967–2988. https://doi.org/10.1007/s11053-020-09655-x.

Cao, Y., Du, Y., Gao, F., Hu, L., Xin, F., Pang, Z., 2012. Origin and evolution of hydrothermal fluids in the Taochong iron deposit, Middle-Lower Yangtze Valley, Eastern China: evidence from microthermometric and stable isotope analyses of fluid inclusions. Ore Geol. Rev. 48, 225–238. https://doi.org/10.1016/j.oregeorev.2012.03.009.

Cao, Y., Du, Y., Pang, Z., Ren, C., Du, Y., Xiao, F., Zhou, G., Chen, J., 2016. Sulfide zonal texture and its geological significance of ores from the Dongguashan copper (gold) deposit in Tongling, Anhui Province, China. Acta Petrol. Sinica 32 (2), 334–350 (in Chinese with English abstract).

Chang, Y., Liu, P., Wu, C., 1991. The Copper-Iron Belt of the Lower and Middle Reaches of the Changjiang River. Geological Publishing House, Beijing, pp. 1–379 (in Chinese with English abstract).

Chelle-Michou, C., Chiaradia, M., Béguelin, P., Ulianov, A., 2015. Petrological evolution of the magmatic suite associated with the coroccohuayco Cu(–Au–Fe) Porphyry-Skarn Deposit, Peru. J. Petrol. 56 (9), 1829–1862.

Chen, Y., Nabelek, P.I., 2017. The influences of incremental pluton growth on magma crystallinity and aureole rheology: numerical modeling of growth of the Papoose Flat pluton, California. Contrib. Mineral. Petrol. 172 (10) https://doi.org/10.1007/s00410-017-1405-6.
Chen, Y.J., Pirajno, F., Wu, G., Qi, J.P., Xiong, X.L., 2012. Epithermal deposits in North Xinjiang, NW China. Int. J. Earth Sci. 101 (4), 889–917.
Chesley, J.T., Halliday, A.N., Snee, L.W., Mezger, K., Shepherd, T.J., Scrivener, R.C., 1993. Thermochronology of the Cornubian batholith in southwest England: implications for pluton emplacement and protracted hydrothermal mineralization. Geochim. Cosmochim. Acta 57 (8), 1817–1835. https://doi.org/10.1016/0016-7037(93)90115-D.
Chicharro, E., Martín-Crespo, T., Gómez-Ortiz, D., López-García, J.Á., Oyarzun, R., Villaseca, C., 2015. Geology and gravity modeling of the Logrosán Sn–(W) ore deposits (Central Iberian Zone, Spain). Ore Geol. Rev. 65, 294–307. https://doi.org/10.1016/j.oregeorev.2014.10.005.
Clarke, D.B., Henry, A.S., White, M.A., 1998. Exploding xenoliths and the absence of 'elephants' graveyards' in granite batholiths. J. Struct. Geol. 20 (9-10), 1325–1343. https://doi.org/10.1016/S0191-8141(98)00082-0.
Cogné, J.P., Perroud, H., 1988. Anisotropy of magnetic susceptibility as a strain gauge in the Flamanville granite, NW France. Phys. Earth Planet. Inter. 51 (4), 264–270.
Coleman, D.S., Gray, W., Glazner, A.F., 2004. Rethinking the emplacement and evolution of zoned plutons: geochronologic evidence for incremental assembly of the Tuolumne Intrusive Suite. Calif. Geol. 32 (5), 433. https://doi.org/10.1130/G20220.110.1130/2004071.
de Saint Blanquat, M., Horsman, E., Habert, G., Morgan, S., Vanderhaeghe, O., Law, R., Tikoff, B., 2011. Multiscale magmatic cyclicity, duration of pluton construction, and the paradoxical relationship between tectonism and plutonism in continental arcs. Tectonophysics 500 (1-4), 20–33.
de Saint-Blanquat, M., Law, R.D., Bouchez, J.-L., Morgan, S.S., 2001. Internal structure and emplacement of the Papoose Flat pluton: an integrated structural, petrographic, and magnetic susceptibility study. GSA Bull. 113, 976–995. https://doi.org/10.1130/0016-7606(2001)113<0976:isaeot>2.0.co;2.
Deng, J., Wang, Q., Huang, D., Wan, L., Yang, L., Gao, B., 2006. Transport network and flow mechanism of shallow ore-bearing magma in Tongling ore cluster area. Sci. China Series D 49 (4), 397–407.
Deng, J., Wang, Q., Xiao, C., Yang, L., Liu, H., Gong, Q., Zhang, J., 2011. Tectonic-magmatic-metallogenic system, Tongling ore cluster region, Anhui Province, China. Int. Geol. Rev. 53 (5-6), 449–476. https://doi.org/10.1080/00206814.2010.501538.
Yangsong, D., 1999. Petrological and mineralogical study of enclaves in plutons in the typical mining districts of Tongling, Anhui and its bearing on the process of magmatism-metallogeny. Chin. J. Geochem. 18 (3), 208–218. https://doi.org/10.1007/BF02831066.
Dunlop, D.J., Özdemir, Ö., Rock Magnetism: Fundamentals and Frontiers. Cambridge: Cambridge University Press; 1997. https://doi.org/10.1017/CBO9780511612794.
Duuring, P., Hagemann, S.G., 2001. A thrust ramp model for gold mineralization at the archean Trondhjemite-hosted Tarmoola deposit: the importance of heterogeneous stress distributions around granitoid contacts. Econ. Geol. Bull. Soc. Econ. Geol. 96, 1379–1396. https://doi.org/10.2113/96.6.1379.
Eldursi, K., Branquet, Y., Guillou-Frottier, L., Marcoux, E., 2009. Numerical investigation of transient hydrothermal processes around intrusions: heat-transfer and fluid-circulation controlled mineralization patterns. Earth Planet. Sci. Lett. 288 (1-2), 70–83. https://doi.org/10.1016/j.epsl.2009.09.009.
Ernst, R.E., Baragar, W.R.A., 1992. Evidence from magnetic fabric for the flow pattern of magma in the Mackenzie giant radiating dyke swarm. Nature 356 (6369), 511–513. https://doi.org/10.1038/356511a0.
Eugster, H.P., 1985. Granites and hydrothermal ore deposits: a geochemical framework. Mineral. Mag. 49 (350), 7–23. https://doi.org/10.1180/minmag.1985.049.350.02.
Ferré, E.C., Bordarier, C., Marsh, J.S., 2002. Magma flow inferred from AMS fabrics in a layered mafic sill, Insizwa, South Africa. Tectonophysics 354 (1), 1–23. https://doi.org/10.1016/S0040-1951(02)00273-1.
Gu, L., Wu, C., Zhang, Z., Pirajno, F., Pei, N., Chen, P., et al., 2011. Comparative study of re-forming fluids of hydrothermal copper-gold deposits in the Lower Yangtze River Valley, China. Int. Geol. Rev. 53, 477–498.
Guo, W., Lu, J., Jiang, S., Zhang, R., Zhao, Z., 2013. Hf isotopes, geochemistry, and petrogenesis of the magmatic rocks in the Shizishan ore field of Tongling, Anhui Province. Sci. China Earth Sci. 56 (6), 993–1013.
He, B., Xu, Y.-G., Paterson, S., 2009. Magmatic diapirism of the Fangshan pluton, southwest of Beijing, China. J. Struct. Geol. 31 (6), 615–626. https://doi.org/10.1016/j.jsg.2009.04.007.
Hedenquist, J.W., Lowenstern, J.B., 1994. The role of magmas in the formation of hydrothermal ore deposits. Nature 370 (6490), 519–527.
Heinrich, C.A., Walshe, J.L., Harrold, B.P., 1996. Chemical mass transfer modelling of ore-forming hydrothermal systems: current practise and problems. Ore Geol. Rev. 10 (3-6), 319–338. https://doi.org/10.1016/0169-1368(95)00029-1.
Holwell, D.A., Keays, R.R., Firth, E.A., Findlay, J., 2014. Geochemistry and mineralogy of platinum group element mineralization in the river valley intrusion, Ontario, Canada: a model for early-stage sulfur saturation and multistage emplacement and the implications for "contact-type" Ni-Cu-PGE sulfide mineralization. Econ. Geol. 109 (3), 689–712. https://doi.org/10.2113/econgeo.109.3.689.
Holzheid, A., Lodders, K., 2001. Solubility of copper in silicate melts as function of oxygen and sulfur fugacities, temperature, and silicate composition. Geochim. Cosmochim. Acta 65 (12), 1933–1951. https://doi.org/10.1016/S0016-7037(01)00545-2.
Hrouda, F., 1982. Magnetic anisotropy of rocks and its application in geology and geophysics. Geophys. Surveys 5 (1), 37–82.
Hrouda, F., Lanza, R., 1989. Magnetic fabric in the Biella and Traversella stocks (Periadriatic Line): implications for the mode of emplacement. Phys. Earth Planet. Inter. 56 (3-4), 337–348.
Hua, R., Chen, P., Zhang, W., Lu, J., 2005. Three major metallogenic events in Mesozoic in South China. Mineral Deposits 24, 99–107.
Huang, S., Xu, Z., Gu, L., 2004. A discussion on geochemical characteristics and genesis of intrusions in Shizishan orefield, Tongling area, Anhui Province. Geol. J. China Univ. 10 (2), 217–226 (in Chinese with English abstract).
Huber, C., Bachmann, O., Vigneresse, J.-L., Dufek, J., Parmigiani, A., 2012. A physical model for metal extraction and transport in shallow magmatic systems. Geochem. Geophys. Geosyst. 13 (8).
Jelínek, V., Kropáček, V., 1978. Statistical processing of anisotropy of magnetic susceptibility measured on groups of specimens. Stud. Geophys. Geod. 22 (1), 50–62.
Kratinová, Z., Závada, P., Hrouda, F., Schulmann, K., 2006. Non-scaled analogue modelling of AMS development during viscous flow: a simulation on diapir-like structures. Tectonophysics 418 (1-2), 51–61.
Lai, J., Chi, G., Peng, S., Shao, Y., Yang, B., 2007. Fluid evolution in the formation of the Fenghuangshan Cu-Fe-Au Deposit, Tongling, Anhui, China. Econ. Geol. 102 (5), 949–970. https://doi.org/10.2113/gsecongeo.102.5.949.
Li, H., Zhang, H., Ling, M.-X., Wang, F.-Y., Ding, X., Zhou, J.-B., Yang, X.-Y., Tu, X.-L., Sun, W., 2011. Geochemical and zircon U-Pb study of the Huangmeijian A-type granite: implications for geological evolution of the Lower Yangtze River belt. Int. Geol. Rev. 53 (5-6), 499–525.
Li, J., Zhang, Y., Dong, S., Johnston, S.T., 2014. Cretaceous tectonic evolution of South China: a preliminary synthesis. Earth Sci. Rev. 134, 98–136. https://doi.org/10.1016/j.earscirev.2014.03.008.
Li, Y., Li, Q.-L., Yang, J.-H., 2019. Tracing water-rock interaction in carbonate replacement deposits: a SIMS pyrite S-Pb isotope perspective from the Chinese Xinqiao system. Ore Geol. Rev. 107, 248–257. https://doi.org/10.1016/j.oregeorev.2019.02.022.
Liang, Q., Jing, H., Gregoire, D.C., 2000. Determination of trace elements in granites by inductively coupled plasma mass spectrometry. Talanta 51, 507–513. https://doi.org/10.1016/S0039-9140(99)00318-5.
Lin, J.-l., Fuller, M., Zhang, W.-Y., 1985. Preliminary Phanerozoic polar wander paths for the North and South China blocks. Nature 313 (6002), 444–449. https://doi.org/10.1038/313444a0.
Liu, G., Yuan, F., Deng, Y., Wang, F., White, N.C., Huizenga, J.M., Li, Y., Li, X., Zhou, T., 2020. Ore-fluid geochemistry of the Hehuashan Pb–Zn deposit in the Tongling ore district, Anhui province, China: evidence from REE and C-H–O isotopes of calcite. Ore Geol. Rev. 117, 103279. https://doi.org/10.1016/j.oregeorev.2019.103279.
Liu, L., Wan, C., Zhao, C., Zhao, Y., 2011. Geodynamic constraints on orebody localization in the Anqing orefield, China: computational modeling and facilitating predictive exploration of deep deposits. Ore Geol. Rev. 43 (1), 249–263. https://doi.org/10.1016/j.oregeorev.2011.09.005.
Liu, L., Zhao, Y., Sun, T., 2012. 3D computational shape- and cooling process-modeling of magmatic intrusion and its implication for genesis and exploration of intrusion-related ore deposits: an example from the Yueshan intrusion in Anqing, China. Tectonophysics 526-529, 110–123.
Liu, L.M., Sun, T., Zhou, R.C., 2014. Epigenetic genesis and magmatic intrusion's control on the Dongguashan stratabound Cu–Au deposit, Tongling, China: evidence from field geology and numerical modeling. J. Geochem. Explor. 144, 97–114. https://doi.org/10.1016/j.gexplo.2014.03.008.
Liu, Z.-f., Shao, Y.-J., Wang, C., Liu, Q.-Q., 2019. Genesis of the Dongguashan skarn Cu-(Au) deposit in Tongling, Eastern China: evidence from fluid inclusions and H-O-S-Pb isotopes. Ore Geol. Rev. 104, 462–476. https://doi.org/10.1016/j.oregeorev.2018.11.021.
Lu, J.J., Hua, R.M., Xu, Z.W., 2003. A two-stage model for formation of the Dongguashan Cu-Au deposit. Geol. J. China Univ. 9, 678–690.
Lü, Q., Qi, G., Yan, J., 2013. 3D geologic model of Shizishan ore field constrained by gravity and magnetic interactive modeling: a case history. Geophysics 78 (1), B25–B35.
Lü, Q., Shi, D., Liu, Z., Zhang, Y., Dong, S., Zhao, J., 2015. Crustal structure and geodynamics of the Middle and Lower reaches of Yangtze metallogenic belt and neighboring areas: insights from deep seismic reflection profiling. J. Asian Earth Sci. 114, 704–716.
Mao, J., Li, X.F., Zhang, Z.H., Wang, Y., Li, H.M., Hu, H.B., 2003. Geology, distribution, types and tectonic settings of Mesozoic epithermal gold deposits in East China. Geol. J. China Univ. 9, 620–637.
Mao, J., Xie, G., Duan, C., Pirajno, F., Ishiyama, D., Chen, Y., 2011. A tectono-genetic model for porphyry–skarn–stratabound Cu–Au–Mo–Fe and magnetite–apatite deposits along the Middle–Lower Yangtze River Valley, Eastern China. Ore Geol. Rev., 43:294-314. https://doi.org/10.1016/j.oregeorev.2011.07.010.
Mao, J.W., Xie, G.Q., Guo, C.L., Yuan, S.D., Cheng, Y.B., Chen, Y.C., 2008. Spatial-temporal distribution of Mesozoic ore deposits in South China and their metallogenic settings. Geol. J. China Univ. 14, 510–526.
Marsh, B.D., 1982. On the mechanics of igneous diapirism, stoping, and zone melting. Am. J. Sci. 282 (6), 808–855.
Matzel, J.E.P., Bowring, S.A., Miller, R.B., 2006. Time scales of pluton construction at differing crustal levels: Examples from the Mount Stuart and Tenpeak intrusions, North Cascades, Washington. GSA Bulletin. 118:1412–30.https://doi.org/10.1130/B25923.1.
McNulty, B.A., Tobisch, O.T., Cruden, A.R., Gilder, S., 2000. Multistage emplacement of the Mount Givens pluton, central Sierra Nevada batholith, California. Geol. Soc. Am. Bull. 112:119-35.https://doi.org/10.1130/0016-7606(2000)112<119:meotmg>2.0.co;2.

Pan, Y., Dong, P., 1999. The Lower Changjiang (Yangzi/Yangtze River) metallogenic belt, east central China: intrusion- and wall rock-hosted Cu–Fe–Au, Mo, Zn, Pb, Ag deposits. Ore Geol. Rev. 15 (4), 177–242. https://doi.org/10.1016/S0169-1368(99)00022-0.

Paterson, S.R., Jr TKF., 1993. Re-examining pluton emplacement processes. J. Struct. Geol. 15:191–206. https://doi.org/10.1016/0191-8141(93)90095-R.

Pina, R., Romeo, I., Ortega, L., Lunar, R., Capote, R., Gervilla, F., Tejero, R., Quesada, C., 2010. Origin and emplacement of the Aguablanca magmatic Ni-Cu-(PGE) sulfide deposit, SW Iberia: a multidisciplinary approach. Geol. Soc. Am. Bull. 122 (5-6), 915–925.

Reynolds, R.R., 1958. Factors controlling the localization of ore deposits in the Shullsburg area, Wisconsin-Illinois zinc-lead district. Econ. Geol., 53:141-63.https://doi.org/10.2113/gsecongeo.53.2.141.

Rochette, P., Jackson, M., Aubourg, C., 1992. Rock magnetism and the interpretation of anisotropy of magnetic susceptibility. Rev. Geophys. 30 (3), 209. https://doi.org/10.1029/92RG00733.

Romeo, I., Tejero, R., Capote, R., Lunar, R., 2008. 3D gravity modelling of the Aguablanca Stock, tectonic control and emplacement of a Variscan gabbronorite bearing a Ni-Cu-PGE ore, SW Iberia. Geol. Mag. 145 (3), 345–359.

Schöpa, A., Annen, C., Dilles, J., Blundy, J., Sparks, S., 2017. Magma emplacement rates and porphyry copper deposits: thermal modeling of the Yerington Batholith, Nevada. Econ. Geol. 112, 1653–1672. https://doi.org/10.5382/econgeo.2017.4525.

Shi, D., Lü, Q., Xu, W., Yan, J., Zhao, J., Dong, S., Chang, Y., 2013. Crustal structure beneath the middle–lower Yangtze metallogenic belt in East China: constraints from passive source seismic experiment on the Mesozoic intra-continental mineralization. Tectonophysics 606, 48–59.

Sillitoe, R.H., 2010. Porphyry copper systems. Econ. Geol. 105 (1), 3–41.

Sun, W., Ding, X., Hu, Y.-H., Li, X.-H., 2007. The golden transformation of the Cretaceous plate subduction in the west Pacific. Earth Planet. Sci. Lett. 262 (3-4), 533–542.

Sun, T., Liu, L., 2014. Delineating the complexity of Cu–Mo mineralization in a porphyry intrusion by computational and fractal modeling: A case study of the Chehugou deposit in the Chifeng district, Inner Mongolia, China. J. Geochem. Explor. 144, 128–143. https://doi.org/10.1016/j.gexplo.2014.02.015.

Tang, Y.C., Wu, Y.C., Chu, G.Z., Xing, F.M., Wang, Y.M., Cao, F.Y., Chang, Y.F., 1998. Geology of Copper-gold Polymetallic Deposits in the Along-Changjiang Area of Anhui Province. Geological Publishing House, Beijing, pp. 1–351 (in Chinese with English abstract).

Tarling, D., Hrouda, F., 1993. Magnetic Anisotropy of Rocks. Springer Science & Business Media.

Thompson, J.F.H., Sillitoe, R.H., Baker, T., Lang, J.R., Mortensen, J.K., 1999. Intrusion-related gold deposits associated with tungsten-tin provinces. Miner. Deposita 34 (4), 323–334.

Tindle, A.G., Pearce, J.A., 1981. Petrogenetic modelling of in situ fractional crystallization in the zoned Loch Doon pluton, Scotland. Contrib. Mineral. Petrol. 78 (2), 196–207.

van der Molen, I., Paterson, M.S., 1979. Experimental deformation of partially-melted granite. Contrib. Miner. Petrol. 70 (3), 299–318.

Vigneresse, J.-L., 2006. Element Mobility in Melts during Successive Intrusions of Crustal-derived Magmas and Sn-W Mineralization. Resour. Geol., 56:293–314. https://doi.org/10.1111/j.1751-3928.2006.tb00285.x.

Vigneresse, J.L., 2007. The role of discontinuous magma inputs in felsic magma and ore generation. Ore Geol. Rev. 30 (3-4), 181–216. https://doi.org/10.1016/j.oregeorev.2006.03.001.

Wang, Q., Deng, J., Huang, D., Xiao, C., Yang, L., Wang, Y., 2011. Deformation model for the Tongling ore cluster region, east-central China. Int. Geol. Rev. 53 (5-6), 562–579.

Wang, Q., Xu, J.-F., Zhao, Z.-H., Bao, Z.-W., Xu, W., Xiong, X.-L., 2004. Cretaceous high-potassium intrusive rocks in the Yueshan-Hongzhen area of east China: Adakites in an extensional tectonic regime within a continent. Geochem. J. 38 (5), 417–434.

Wang, S.-W., Zhou, T.-F., Yuan, F., Fan, Y., Zhang, L.-J., Song, Y.-L., 2015. Petrogenesis of Dongguashan skarn-porphyry Cu-Au deposit related intrusion in the Tongling district, eastern China: Geochronological, mineralogical, geochemical and Hf isotopic evidence. Ore Geol. Rev. 64, 53–70.

Wei, W., Martelet, G., Le Breton, N., Shi, Y., Faure, M., Chen, Y., Hou, Q., Lin, W., Wang, Q., 2014. A multidisciplinary study of the emplacement mechanism of the Qingyang-Jiuhua massif in Southeast China and its tectonic bearings. Part II: Amphibole geobarometry and gravity modeling. J. Asian Earth Sci. 86, 94–105. https://doi.org/10.1016/j.jseaes.2013.09.021.

Wu, C., Dong, S., Robinson, P.T., Frost, B.R., Gao, Y., Lei, M., Chen, Q., Qin, H., 2014. Petrogenesis of high-K, calc-alkaline and shoshonitic intrusive rocks in the Tongling area, Anhui Province (eastern China), and their tectonic implications. Geol. Soc. Am. Bull. 126 (1-2), 78–102.

Wu, C.L., Dong, S., Guo, H.P., Guo, X.Y., Gao, Q.M., Liu, L.G., et al., 2008. Zircon SHRIMP U-Pb dating of intermediate-acid intrusive rocks from Shizishan, Tongling and the deep processes of magmatism. Acta Petrol. Sinica. 24, 1801–1812.

Wu, C.L., Gao, Q.M., Guo, H.P., Guo, X.Y., Liu, L.G., Gao, Y.H., et al., 2010. Petrogenesis of the intermediate-acid intrusive rocks and zircon SHRIMP dating in Tongling, Anhui. China. Acta Petrol. Sinica. 26, 2630–2652.

Xie, J., Wang, Y., Li, Q., Yan, J., Sun, W., 2018. Petrogenesis and metallogenic implications of Late Mesozoic intrusive rocks in the Tongling region, eastern China: a case study and perspective review. Int. Geol. Rev. 60 (11–14), 1361–1380. https://doi.org/10.1080/00206814.2017.1386130.

Xie, J., Yang, X., Sun, W., Du, J., 2012. Early Cretaceous dioritic rocks in the Tongling region, eastern China: Implications for the tectonic settings. Lithos 150, 49–61.

Xie, J., Yang, X., Sun, W., Du, J., Xu, W., Wu, L., Wang, K., Du, X., 2009. Geochronological and geochemical constraints on formation of the Tongling metal deposits, middle Yangtze metallogenic belt, east-central China. Int. Geol. Rev. 51 (5), 388–421.

Xu, X., Lu, S., Xie, Q., Bai, L., Chu, G., 2008. SHRIMP zircon U-Pb dating for the magmatic rocks in Shizishan Ore-field of Tongling, Anhui Province, and its geological implications. Acta Geol. Sin. 82, 500–509.

Xu, X.C., Fan, Z.L., He, J., Liu, X., Liu, X.Y., Xie, Q., et al., 2014. Metallogenic model for the copper-gold-polvmetallic deposits in Shizishan ore-field, Tongling, Anhui Province. Acta Petrol. Sinica 30, 1054–1074.

Xu, X.C., Yin, T., Lou, J.W., Lu, S.M., Xie, Q., Chu, P.L., 2010. Origin of Dongguashan stratabound Cu-Au skarn deposit in Tongling: restraints of sulfur isotope. Acta Petrol. Sinica 26, 2739–2750.

Xu, Z., Lu, X., Ling, H., Lu, J., Jiang, S., Ni, P., Huang, S., Hua, M., 2005. Metallogenetic mechanism and timing of late superimposing fluid mineralization in the Dongguashan Diplogenetic Stratified Copper Deposit, Anhui Province. Acta Geol. Sinica – English Edition 79 (3), 405–413. https://doi.org/10.1111/j.1755-6724.2005.tb00906.x.

Yang, S.-Y., Jiang, S.-Y., Li, L., Sun, Y., Sun, M.-Z., Bian, L.-Z., Xiong, Y.-G., Cao, Z.-Q., 2011. Late Mesozoic magmatism of the Jiurui mineralization district in the Middle-Lower Yangtze River Metallogenic Belt, Eastern China: precise U-Pb ages and geodynamic implications. Gondwana Res. 20 (4), 831–843. https://doi.org/10.1016/j.gr.2011.03.012.

Yang, X.-Y., Lee, I., 2011. Review of the stable isotope geochemistry of Mesozoic igneous rocks and Cu–Au deposits along the middle–lower Yangtze Metallogenic Belt, China. Int. Geol. Rev. 53 (5-6), 741–757.

Zhai, Y.S., Yao, S.Z., Lin, X.D., Zhou, X.N., Wan, T.F., Jin, F.Q., et al., 1992. Fe-Cu (Au) Metallogeny of the Middle-Lower Changjiang Region. Geological Publishing House.

Zhang, L., Zhou, T., Yuan, F., Fan, Y., Cooke, D.R., 2011. Petrogenetic–metallogenetic setting and temporal–spatial framework of the Yueshan district, Anhui Province, east-central China. Int. Geol. Rev. 53 (5-6), 542–561.

Zhao, C., Hobbs, B.E., Ord, A., 2010. Theoretical and numerical investigation into roles of geofluid flow in ore forming systems: integrated mass conservation and generic model approach. J. Geochem. Explor. 106 (1-3), 251–260.

Zhao, X., Coe, R.S., 1987. Palaeomagnetic constraints on the collision and rotation of North and South China. Nature 327 (6118), 141–144.

Zhou, T., Wang, S., Fan, Y., Yuan, F., Zhang, D., White, N.C., 2015. A review of the intracontinental porphyry deposits in the Middle-Lower Yangtze River Valley metallogenic belt, Eastern China. Ore Geol. Rev., 65:433–56.https://doi.org/https://doi.org/10.1016/j.oregeorev.2014.10.002.

Zhou, T., Yuan, F., Yue, S., Liu, X., Zhang, X., Fan, Y., 2007. Geochemistry and evolution of ore-forming fluids of the Yueshan Cu–Au skarn-and vein-type deposits, Anhui Province, South China. Ore Geol. Rev. 31 (1-4), 279–303. https://doi.org/10.1016/j.oregeorev.2005.03.016.

Zhou, T., Yuan, F., Yue, S., Zhao, Y., 2000. Two series of copper-gold deposits in the middle and lower reaches of the Yangtze River area (MLYRA) and the hydrogen, oxygen, sulfur and lead isotopes of their ore-forming hydrothermal systems. Sci. China, Ser. D Earth Sci. 43 (S1), 208–218. https://doi.org/10.1007/BF02911946.